https://doi.org/10.15407/ufm.21.04.580

T.M. RADCHENKO *, **O.S. GATSENKO,**
V.V. LIZUNOV, and V.A. TATARENKO **
G.V. Kurdyumov Institute for Metal Physics of the N.A.S. of Ukraine,
36 Academician Vernadsky Blvd.,
UA-03142 Kyiv, Ukraine
* tarad@imp.kiev.ua, ** tatar@imp.kiev.ua

MARTENSITIC α''-$Fe_{16}N_2$-TYPE PHASE OF NON-STOICHIOMETRIC COMPOSITION: CURRENT STATUS OF RESEARCH AND MICROSCOPIC STATISTICAL-THERMODYNAMIC MODEL

The literature (experimental and theoretical) data on the tetragonality of martensite with interstitial–substitutional alloying elements and vacancies are reviewed and analysed. Special attention is paid to the studying the martensitic α''-$Fe_{16}N_2$-type phase with unique and promising magnetic properties as an alternative to the rare-earth intermetallics or permendur on the world market of the production of permanent magnets. The period since its discovery to the current status of research is covered. A statistical-thermodynamic model of 'hybrid' interstitial–substitutional solid solution based on a b.c.t. crystal lattice, where the alloying non-metal constituents (impurity atoms) can occupy both interstices and vacant sites of the host b.c.c.(t.)-lattice, is elaborated. The discrete (atomic-crystalline) lattice structure, the anisotropy of elasticity, and the 'blocking' and strain-induced (including 'size') effects in the interatomic interactions are taken into account. The model is adapted for the non-stoichiometric phase of Fe–N martensite maximally ordered by analogy with α''-$Fe_{16}N_2$, where nitrogen atoms are in the interstices and at the sites of b.c.t. iron above the Curie point. It is stressed an importance of adequate data on the available (in the literature) temperature- and concentration-dependent micro-scopic energy parameters of the interactions of atoms and vacancies. The features of varying (viz. non-monotonic decreasing with increasing temperature) the relative concentration of N atoms in the octahedral interstices of b.c.t. Fe, and therefore, the degree of its tetragonality (correlating with this concentration) are elucidated. Within the wide

Citation: T.M. Radchenko, O.S. Gatsenko, V.V. Lizunov, and V.A. Tatarenko, Martensitic α''-$Fe_{16}N_2$-Type Phase of Non-Stoichiometric Composition: Current Status of Research and Microscopic Statistical-Thermodynamic Model, *Progress in Physics of Metals*, **21**, No. 4: 580–618 (2020)

range of varying the total content of introduced N atoms, the ratio of the equilibrium concentration of residual site vacancies to the concentration of thermally activated vacancies in a pure b.c.c. Fe is demonstrated at a fixed temperature.

Keywords: α″-$Fe_{16}N_2$ phase, Fe–N martensite, interstitial–substitutional solid solution, tetragonality, vacancies, atomic ordering, rare-earth-free magnetic materials, permanent magnets.

1. Introduction

1.1. Rare-Earth-Free Materials for Permanent Magnets

It is currently known [1, 2] that permanent magnets are one of the strategic metal-based products in the world industry due to a wide range of their applications: from micro-electromechanical and nano-electromechanical systems to high-power electricity generators using many tons of magnetic materials containing critical rare-earth metals. Such non-renewable elements are the main factor that constrains or increases the cost of fabrication of magnetic products. So far, there is no alternative to permanent magnets based on rare-earth intermetallics of the Sm–Co or Nd–Fe–B systems as well as based on the permendur (*e.g.*, of the $Fe_{65}Co_{35}$ composition). China is currently the absolute monopolist in the market of rare-earth metals as the raw materials for such magnetic products [3, 4]. Therefore, the task of obtaining new permanent magnets, which have comparable characteristics to existing magnets, but free from critical elements (such as rare-earth metals), is extremely important for industrial and national securities. In addition, our industrial society requires a new energy concept with an ever-increasing emphasis on improving the efficiency of electricity transmission and utilization [5–7]. Since magnetic materials are essential for magnetic devices, any improvement in magnetic materials could have a significant impact on energy resources and applications [1].

The new tailored metallic phases do not containing critical elements (non-renewable on the Earth) may act as an alternative to the permendur and rare-earth permanent magnets. The materials with interesting thermo- and magnetomechanical (and magnetoelectric) effects are, *e.g.*, well-known $L1_0$-Fe–Ni-type elinvars with rather tetragonal crystal lattice (but not cubic one due to the layered atomic ordering [8–10]) and cubic $L1_2$-Fe–Ni-type invars [11–14]. Due to their properties, they successfully complement a series of the best rare-earth intermetallics and permendur (*e.g.*, b.c.c.-lattice-based $Fe_{65}Co_{35}$), which possesses very high magnetic saturation levels (at 2.45 T [15]). Such metallic phases (particularly known as tetrataenite) are present in the meteorites, but their synthesis is very difficult in the Earth conditions.

During past five–seven years, a great progress in the world has been made toward studying and feasible improving the microstructure and physical properties of non-rare-earth materials for permanent magnets [1, 2]. Researchers investigated several new materials-candidates. Some of them have showed realistic potential for replacing rare-earth permanent magnets for some applications [1, 2]. Properties of these materials are described in dozens and even hundreds of published research articles and several reviews. In the recent review [2], authors addressed about such systems as Mn-based Mn–Al and Mn–Bi alloys with high magnetocrystalline anisotropy, spinodally decomposing Fe-based Al-, Ni-, Co-containing (Alnico) alloys, high-coercivity tetrataenite $L1_0$-phase in Fe–Ni and Fe–Co, Co-rich $HfCo_7$ and Zr_2Co_{11} intermetallic compounds, Co_3C and Co_2C carbides, and iron nitride α''-$Fe_{16}N_2$. The latter system attracts a considerable interest due to its exceptionally high saturation magnetization, low cost of Fe, and because its elements are the most earth abundant among all magnetic materials [2].

1.2. Discovery of α''-$Fe_{16}N_2$ and Its Large Saturation Magnetization

A chemically ordered nitride α''-$Fe_{16}N_2$ was discovered and characterized structurally by Kenneth Henderson Jack in his classical works in 1951 [16, 17]. The magnetic α''-$Fe_{16}N_2$-type phase of Fe–N-martensite has the largest saturation magnetic-field strength (2.58 T [18], 2.6–2.8 T [19], 2.83 T [20], 2.9 T [21], 3.1 T [22]) far beyond the iron–cobalt alloy and all other magnetic materials. The α''-$Fe_{16}N_2$ can possess even an ultralow positive temperature coefficient of coercivity (within the range from 300 K to 425 K) [23]. To explain the giant saturation magnetization behaviour in α''-$Fe_{16}N_2$, a 'cluster + atom' model was proposed [24]. This model is associated with partially localized electron states. Two years later, the partial localization behaviour of $3d$-electrons in α''-$Fe_{16}N_2$ was confirmed by means of the x-ray magnetic circular dichroism (XMCD) measurements [25]. Generally, the origin of the giant magnetic moment can be attributed to both the intrinsic effects such as partial localization of d-electrons in the Fe_6N octahedrons and the nature of the exchange interaction promoting the high-spin states through Hund's coupling [26]. The double-exchange interaction is the strongest and favours a high-spin state. The presence of the super-exchange interaction between the Fe sites within the Fe_6N octahedral region indicates the existence of localized states, which may also contribute to the occurrence of a giant moment in this material [26].

1.3. Fabrication Methods and Structure

The earliest and commonly used so far method to prepare mainly a bulk (and rarely, thin film) α''-$Fe_{16}N_2$ material is the process of nitriding, quenching, and annealing. The reaction–transformation sequence of

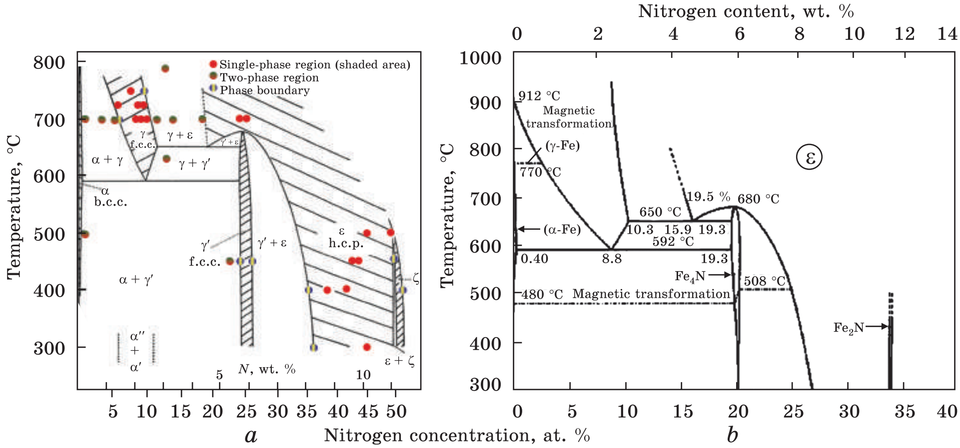

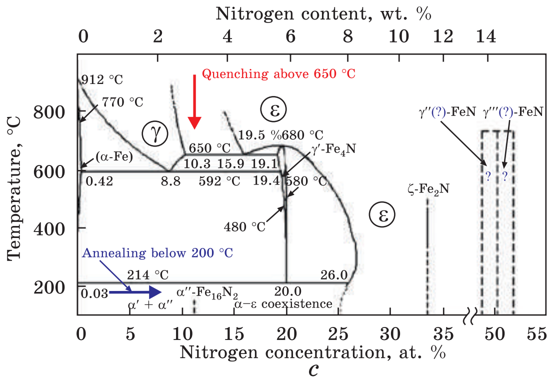

Fig. 1. The iron–nitrogen phase diagrams adopted from different references [16, 29, 30] (*a*–*c*). Bold (coloured) vertical and horizontal arrows (*c*) [30] depict two methods for reaching α″-Fe$_{16}$N$_2$: either from top to bottom (typical for bulk samples) or from left to right below 214 °C (most used for thin films

this method includes four different phases (α, γ, α′, α″) and three phase transformations (including γ→α′ martensitic one, which proceeds by shear without diffusion) [27, 28] (see also Fig. 1 [16, 29, 30]):

$$\alpha\text{-Fe} \xrightarrow[\approx 700-750\ ^{\circ}\mathrm{C}]{\text{nitriding}} \gamma\,\text{Fe–N austenite} \xrightarrow[<0\ ^{\circ}\mathrm{C}]{\text{quenching}}$$

$$\alpha'\text{Fe–N martensite} \xrightarrow[\approx 120-150\ ^{\circ}\mathrm{C}]{\text{tempering}} \alpha''\text{-Fe}_{16}\text{N}_2.$$

Here, at ≅750 °C, α-Fe is subjected to the nitriding procedure to form a nitrogen austenite phase, which then quenched below 0 °C in order to obtain a martensitic α′-phase; then, it is annealed at ≅120 °C (370–420 K) for ≈1–2 hours to obtain α″-Fe$_{16}$N$_2$ phase [27, 28], where N atoms have an ordered distribution.

There are also several other methods to prepare α″-Fe$_{16}$N$_2$. They are as follow: the molecular beam epitaxy [31, 32], the ion implantation [33–35] and beam deposition [36, 37], the facing target [38–40] and reactive (magnetron) [41–43] sputtering, the ball milling [44], and so-called ‘strained-wire method’ [1, 45] when a uniaxial tensile stress is applied on the wire-shaped sample during the post-annealing stage.

In spite of the discovery in the middle of the last century, the magnetic behaviour of the α''-$Fe_{16}N_2$ phase remained a mystery over a period of 40 years. This is due to the questionable and even controversial results in a series of works concerning the saturation magnetization values. The article of Kim and Takahashi in 1972 [18] reported on high magnetization in α''-$Fe_{16}N_2$ has inspired many groups of scientists all over the world to explore the material. Motivated and encouraged by the promising magnetic properties that α''-$Fe_{16}N_2$ phase demonstrates, researchers undertook quite a few attempts to study theoretically and experimentally this phase and prepare (through different synthesis techniques) the samples with as possible larger its volume fraction [46–58] (see also references in recent reviews [1, 2]).

Actually, the α''-$Fe_{16}N_2$ structure is difficult for preparation and mass production. This structure is a metastable [59, 60]: at temperatures of >463 K [61] (but no higher than 523 K [62]) and with time (years) [63], it decomposes according to the decomposition reaction [61, 63]:

$$\alpha''\text{-}Fe_{16}N_2 \rightarrow 8(\alpha\text{-}Fe) + 2(\gamma'\text{-}Fe_4N).$$

So, in other words, the decomposition reaction that occurs in tempered Fe–N martensite leads to the formation of ordered nitride precipitates, namely, the b.c.c.-based ordered nitride α''-$Fe_{16}N_2$ further transformed into another f.c.c.-based nitride γ'-Fe_4N [17].

Note that literature data on the decomposition temperature of α''-$Fe_{16}N_2$ strongly differ from ≈463 K to ≈673 K. To affect (improve) the thermal stability and soft magnetic problems, the adding a small amount of third element has been proposed: Ni [64, 65], Cu [64], V [64], Cr [64, 66], Al [66, 67], Ti [64, 68, 69], Mn [64, 66, 70], Co [64, 69–72], H [71], Bi, [72], Sb [72], Pt [72], Ta [73–76], W [73], Zr [75, 76], Nb [75, 76], Hf [75]. However, the doping (alloying) may degrade some other magnetic characteristics [73]. For example, a giant magnetic effect was not revealed in the sponge-like bulk α''-$Fe_{16}N_2$ contaminated with oxygen impurity [77].

In addition to the metastability, the obtaining of α''-$Fe_{16}N_2$ is complicated by a wide variety of compounds detectable in the binary Fe–N system (see Fig. 1). Besides the α''-$Fe_{16}N_2$, they are as follow: b.c.t.-based α'-Fe_8N, f.c.c.-based γ'-Fe_4N, h.c.p.-based ε-Fe_3N, orthorhombic-based ζ-Fe_2N, (hypothetical) f.c.c.(?)-based FeN [78, 79], and tentative γ''-Fe_8N_2 of tetragonal symmetry [80]. Nevertheless, in the literature, there are quite a lot of works, where authors claim on the synthesis of α''-$Fe_{16}N_2$ phase mainly in (thin) films, rarer in bulk materials, powders, (nano)composites, (nano)particles, and (nano)ribbons.

Vertical and horizontal (coloured) arrows in Fig. 1, *c* show two most often used methods to obtain the α''-$Fe_{16}N_2$ phase. The 'top-to-down' (red) arrow denotes the quenching method (firstly used by Jack [17]),

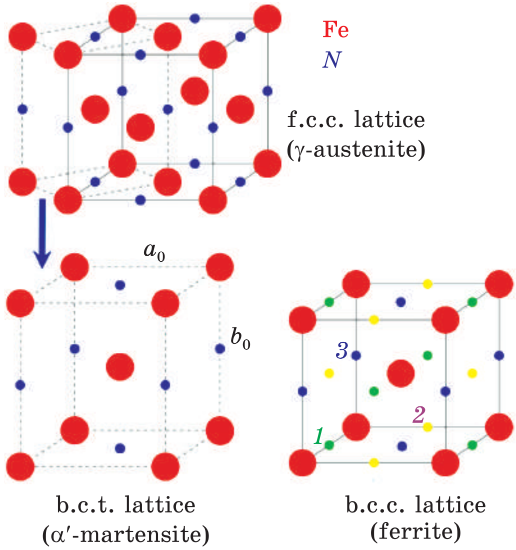

Fig. 2. Octahedral interstitial sites (small circles) in f.c.c. structure (top) and their positions in b.c.t. structure (with lattice parameters a_0 and b_0) after the martensitic transformation (bottom left). Three (*1*–*3*) types of octahedral interstices in b.c.c. structure (bottom right). Schematic (f.c.c., b.c.c., and b.c.t.) structures are adopted from Ref. [81]

which includes nitriding, quenching, and annealing steps (according to the transformation reaction mentioned at the beginning of this subsection). During the nitriding step, the γFe–N austenite forms with a random distribution of N atoms over the octahedral interstices of f.c.c. lattice (Fig. 2, top). After the rapid quenching, the high-temperatures austenitic f.c.c. phase transform into the b.c.c. (more precisely, b.c.t.) structure with N atoms 'frozen' at the interstitial sites since they (N atoms) have no time to move from the interstices occupied in the austenite, and the additional interstitial holes created by the f.c.c. → b.c.c. (b.c.t.) transformation remain empty [27, 28]. As a result, a b.c.t. structure of the same composition as the parent austenite is formed; this phase is known as α′Fe–N martensite (Fig. 2, bottom left). The tetragonality of this martensite lattice is a direct consequence of the preferred occupation of one of the three possible interpenetrating sublattices of octahedral interstices in b.c.c. lattice (Fig. 2, bottom right) [81].

This circumstance, when the impurity N atoms occupying the octahedral interstices of f.c.c. lattice fall into only one sublattice of octahedral interstices in the b.c.c.(t.) phase and thus cause the tetragonal distortions with corresponding lattice-parameter ratio b_0/a_0 (see Fig. 2), is similar to C atoms in α-Fe [81] and known as Bain's transformation [82, 83] from f.c.c.-austenite to b.c.c.-ferrite.

We can also interpret it as a result of a special type of atomic ordering, when at low temperatures, below the temperature of the martensitic transformation, the occupation of only one sublattice of octahedral interstices (O_z interstices) by impurity atoms becomes strongly energy-preferable. In other words, the martensitic transformation occurring through a displacive (diffusionless) mechanism without redistribution of impurity N atoms can be viewed as a special type of 'orientational'-ordering transition [81].

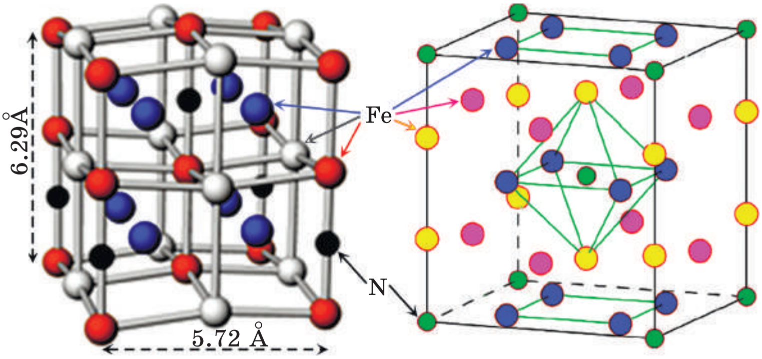

Fig. 3. Structure of α''-$Fe_{16}N_2$ (adopted from Refs. [17, 20]). Left and right unit cells are crystallographically equivalent; each of them contains 16 Fe- and 2 N-atoms

Prolonged annealing (tempering) of the α'-phase upon suitable heat-treatment temperature (≈370–420 K) and at a specific stoichiometry (Fe/N = 8/1) leads to the ordering of nitrogen atoms and appearing the ordered iron–nitrogen martensite α''-$Fe_{16}N_2$ (Fig. 3). Its unit cell comprises eight distorted b.c.c. cells of α-Fe, where N atoms occupy two of 48 available octahedral interstitial sites in a perfectly ordered manner, *i.e.*, two of the 16 O_z interstices, whereas the 16 O_x and 16 O_y interstices virtually always completely empty. The lattice parameters are 5.72 Å and 6.292 Å [17, 27, 28] as shown in Fig. 3, left. It is importantly that the b.c.c. Fe cells are deformed, since there are filled and unfilled octahedrons in the structure. If the hole (centre of octahedron) is occupied by N atom (as depicted in Fig. 3, right), two (upper and lower) Fe atoms are shifted from N atom in the opposing directions along the vertical (z) line (axis). When the hole is empty, the Fe atoms occupy the same positions as in the α-Fe lattice.

In other words, according to K.H. Jack [17], the structure of the α''-$Fe_{16}N_2$ phase may be interpreted [92] as tetragonal interstitial superlattice within the b.c.c. host lattice of α-Fe with the N atoms making up a nearly double-period b.c.c. lattice within the O_z sublattice of octahedral interstices, with $a = c \approx 2a_0 \cong b$, where a_0 is the b.c.c. crystal lattice parameter of the b.c.c. host lattice of α-Fe. So, the crystal lattice parameters of the α''-$Fe_{16}N_2$ phase are as follow:

$$a_{\alpha''} \approx 2a_0 = 2\times 2.86\ \text{Å} = 5.72\ \text{Å},\ b_{\alpha''} = 6.229\ \text{Å} \cong 2a_0.$$

It should be emphasise that the spacing $a_{\alpha''}$ of the tetragonal α''-$Fe_{16}N_2$ phase is almost exactly equal to twice the crystal lattice parameter of the parent phase (α-Fe).

Note also that the filled NFe_6 octahedrons (as that in Fig. 3, right) have almost same size in all the Fe–N phases: α, α', α'', γ, γ'; however, their numbers and distribution are different [27, 28].

The 'left-to-right' (blue) arrow in Fig. 1, *c* shows another way for generating α″-$Fe_{16}N_2$ phase, which is commonly used to prepare this phase in thin films. A mixture of Fe and N atoms with a fixed atomic fraction has to be generated through the plasma or sputtering method in a high vacuum and then deposited on a single-crystalline substrate. A lattice mismatch between the substrate and the deposited Fe–N film cause the strain effect, which results in the martensitic α′-Fe_8N phase. Then, after a post-annealing process below 214 °C in a vacuum, the α′-Fe_8N phase transform into the α″-$Fe_{16}N_2$ phase with an ordered distribution of N atoms.

Among dozens of articles, only a few works claimed pure α″-$Fe_{16}N_2$ phase preparation. Commonly, the prepared Fe–N samples consist of several possible phases with a partial volume ratio of an α″-$Fe_{16}N_2$ phase inside, but just a volume fraction of this phase defines magnetic properties: the higher volume fraction, the better properties [22, 84, 85]. In this respect, a key parameter to evaluate the quality of the prepared compound and its magnetic properties is information on the volume ratio of α″-$Fe_{16}N_2$ phase. To evaluate the amount of this phase in the prepared Fe–N system, the x-ray diffraction (XRD) technique is most commonly used [16–18, 21, 22, 38, 39, 47, 50, 53, 54, 56]. However, a new method based on the analysis of the x-ray photoelectron spectra (XPS) was also used [84]. Both methods provide the same volume ratio values for the phase fraction within the reasonable error region.

1.4. Motivation of the Study

Crucial properties of permanent magnets (both already widely used and acting as potential candidates), particularly, coercivity and permanent magnetization, strongly depend on (micro)structure. That is why deep understanding metallurgical processing, phase stability and (micro) structural changes is major for designing and improving permanent magnets as well as prediction their properties [1, 2].

The key factors, which practically determine the phase magnetization, are external impacts (particularly, strain and temperature), interatomic interactions, and order in the spatial distribution of N atoms, which can occupy both octahedral interstices and metal-lattice sites with vacancies. Redistribution of N atoms results to partial (dis)ordering, the degree of which correlates with a magnetization value: the latter increases (decreases) as the atomic long-range order parameter increases (decreases) [86].

Note that, so far, many research groups, including experimentalists and theoreticians cannot reproduce or justify such unique magnetic characteristics of the α″-$Fe_{16}N_2$. After symposium on a topic of $Fe_{16}N_2$ at the Annual Conference on Magnetism and Magnetic Materials in 1996, where there was no a decisive conclusion on the giant saturation magnetization origin, this research topic has been dropped by most magnetic researchers. To this day, therefore, there is no a complete understanding and explanation of the magnetism of α''-$Fe_{16}N_2$ phase. Thus, this problem remains a topical and motivated, and even somewhat a mystery.

Currently, there is a lack of full understanding of how we can change the external thermodynamic parameters (temperature, pressure or deformation) and regulate the structure, thereby the properties of magnetic α''-$Fe_{16}N_2$-type martensite. To overcome such a theoretical gap, we are motivated in the development of the microscopic model of a 'hybrid' solid solution, in which the interstitial non-metal atoms from octahedral interstices can partially move to the sites of b.c.c. (or tetragonal) lattice of metal with vacancies. At that, we have to take into account the discrete (atomic-crystalline) structure of the lattice, its elastic and magnetocrystalline anisotropy as well as the effective interatomic interactions of all atoms (not only the nearest or several neighbouring).

2. Statistical-Thermodynamic Model of Solid Solution of N Atoms in the Interstices and Sites of B.C.C.(T.)-Fe with Vacancies

2.1. Geometry of Solid-Solution Lattice and General Reasonable Assumptions

Binary solid solutions are commonly considered to belong to one of two 'geometrical'-model categories, which are described as either interstitial or substitutional. However, currently it is quite clear that this simple differentiation is an approximation; in reality, solute atoms occupy both the lattice solvent-atom sites and one or more subsets of interstitial sites. Though the vast majority of solute (impurity) atoms in the overwhelming majority of solid solutions are located only in one subset of geometrically equivalent sites, this is not always the case. There are solutions, where significant fractions of impurity atoms reside in both interstitial and substitutional positions (within the wide temperature ranges). The iron–boron and metal–helium systems act as an example of such solutions [87, 88].

It is known from the literature that there is a viewpoint that the anomaly of the temperature dependence of the lattice-parameters' ratio (tetragonality degree) of (irradiated) b.c.c.(t.) α'-martensite is caused by a peculiar phase transformation, *e.g.*, impurity C atoms from octahedral interstices are 'captured' by vacant sites of b.c.c.(t.) Fe lattice (see Refs. [89–92] and references therein). Actually, we can assume that this feature ('capture') is proper for not only irradiated martensites, but also may occur in any (realistic) imperfect interstitial solid solution (al-

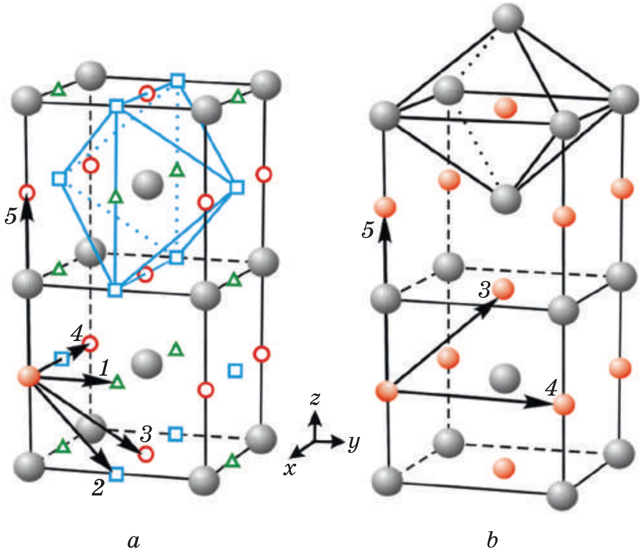

Fig. 4. The b.c.c. lattice structure (adopted from Ref. [95]) comprising (*a*) three interpenetrating (also b.c.c.) sublattices of octahedral interstices (open circles, triangles, squares) within the Fe host lattice (grey balls), and (*b*) only one octahedral sublattice occupied by impurity atoms (small balls). Arrows indicate the first five coordination shells for interstitial impurities

loy) that contains the vacant sites. For instance, in Ref. [93], authors consider $L1_2$-type superstructures, where the changes in the long-range order parameter relate to the introduction ('deposition') of deformation-induced interstitial atoms into vacant sites. The attempt to design a simple model of binary hybrid interstitial–substitutional solid solution have been also considered in Ref. [94], where, however, the author has ignored the lattice uniform dilation effects and restricted the case to sufficiently low solute contents.

In this section, we develop the model of diluted macroscopically homogeneous solid solution, where isolated impurity atoms of non-metal element (X) may occupy both octahedral interstices (i) and vacant sites (s) of metal (Me) b.c.c.(t.) lattice (Fig. 4 [95]). In a general case, there is no a reason to deny that one (and the same) site can 'capture' simultaneously several X atoms [96] with the formation of their 'complexion' [97]. The total number of such atoms within the 'complexions' can be roughly estimated, *e.g.*, from the condition of closeness to zero of the total 'elastic power' of the resulting restricted defect 'vacant site + complexion' (as a centre of 'pure' dilatation) and/or partial removal of mechanical stresses and, thus, a decrease in the elastic energy of the solid solution. However, in this work (as a first step), for simplicity, we will neglect the formation of such complexes, which are less favourable by entropy [97] than the single impurity atoms. We will take into account the presence of excess monovacancies (v) at the b.c.c.(t.)-Me sites, and assume that, in the equilibrium state, X atoms practically do not jump into the cramped tetrahedral interstices as well as Me ions practically do not jump from the sites to comparatively cramped interstices.

In order to study the temperature- and concentration-dependent characteristics of the redistribution of interacting impurity X atoms, we assume so-called dynamic equilibrium, when a quasi-local thermodynamically quasi-equilibrium distribution of impurity atoms already occurred in the temperature and pressure ranges we study. Such an equilibrium distribution 'adapt' to the often non-equilibrium distribution of unoccupied sites v. The character of the spatial distribution of the unoccupied sites v varies rather slowly with time. At that, the entire system ('hybrid' solid solution) may already be close to equilibrium relative to the diffusion 'suction' of excess vacancies v from the 'vacuum' into the Me crystal (or their leaving it). This assumption is justified by the kinetic features of the process of redistribution of impurity atoms from the interstitial sites to the sites (such features manifest themselves most fully in the case when the sites are energetically more advantageous even for a non-metal X, at least, for its low concentration inside the host metal Me). Impurity X atoms move from i positions to s positions as a result of mutual 'search' for some interstitial X atom and some vacant v site. This occurs mainly through the 'fast' interstitial migration of impurity atoms rather than the 'slow' bulk diffusion of vacancies.

However, we have to note that the transfer of part of X atoms onto the sites caused by their tendency to increase the entropy of the system cannot decrease the number of the equilibrium thermally activated vacancies. If even some of X atoms occupied some part of a great number of site vacancies, in an equilibrium state, at least no less number of new vacancies appears. In turn, this means that, in this case, the overwhelming majority of X atoms transferred to sites are located at sites previously occupied by Me ions, but which became vacant as a result of the completion of the Me site lattice, stimulated by the presence of interstitial X atoms. The latter effect has not only a 'statistical' cause (due to the entropic factor), but also the 'force' one. Therefore, it can manifest itself even at low temperatures and low X contents, especially, if the intracrystalline (force) field, generated in the sites by the interstitial atoms, is microscopically inhomogeneous, and therefore, an energy factor associated with the inhomogeneity of this field is significant. Note that such a field modulation can be realized even for a macroscopically uniform spatial distribution of interstitial X atoms. Particularly, when they act on Me (as well as X) atoms in the neighbouring sites with energies comparable to the energy of sublimation, *e.g.*, by the type of 'blocking' [89, 98] when it is not compensated by the bulk deformation effects.

Since Fe–N acts as an object of the study in this work, we draw the reader's attention to further two designations in the text and equations: X = N and Me = Fe.

2.2. Occupation-Probability Functions and Configurational Free Energy

Let us $c^{\alpha}(\mathbf{R})$ ($c_p^{\beta}(\mathbf{R})$) is a random quantity, which equals to 1 if a site with radius-vector $\mathbf{R}$ (interstice with radius-vector $\mathbf{R} + \mathbf{h}_p$ in a primitive unit cell $\mathbf{R}$) is occupied by an 'atom' of kind α = Fe, N_s, υ (is occupied by an 'atom' of kind $\beta = N_i, \varnothing$), and 0 otherwise (if not). Here, N_s and N_i denote the nitrogen atoms substituting sites s and octahedral interstices i in the b.c.c.(t.) Fe, respectively. To model the excess monovacancies on the sites or remaining unoccupied octahedral interstices, we consider them as 'atoms' of additional 'substitutional' (υ) or 'interstitial' ($\varnothing$) constituents, respectively. A set of octahedral interstices in the b.c.c. Fe consists of three interpenetrating sublattices $\{\mathbf{R} + \mathbf{h}_p\}$, where p = 1, 2, 3 (see Fig. 4). Each sublattice numbered with p = 1, 2, 3 is isostructural to the 'mean' b.c.c. lattice of N_s sites $\{\mathbf{R}\}$ and displaced (as a whole) with respect to the origin site of cubic conventional unit cell of b.c.c. crystal by the vector

$$\mathbf{h}_1 = \frac{a_0}{2}(1;\ 0;\ 0),\ \ \mathbf{h}_2 = \frac{a_0}{2}(0;\ 1;\ 0),\ \ \mathbf{h}_3 = \frac{a_0}{2}(0;\ 0;\ 1),$$

respectively, in a crystalline-physical system of coordinates, $Oxyz$, where a_0 is the basic parameter of impurity-free unit cell (see Fig. 4). By the definition, $P^{\alpha}(\mathbf{R}) \equiv \langle c^{\alpha}(\mathbf{R})\rangle$ and $P_p^{\beta}(\mathbf{R}) \equiv \langle c_p^{\beta}(\mathbf{R})\rangle$ are single-site probabilities to find atoms α and β kind in the site $\mathbf{R}$ and the interstice $\mathbf{R} + \mathbf{h}_p$, respectively, and symbol $\langle\ldots\rangle$ denotes the statistical averaging over all permitted atomic configurations in case of their canonical distribution. We assume a self-consistent mean field approximation (neglecting correlation) without limiting an interatomic-interaction radius [89, 92], *i.e.*, take into account interatomic interactions in all coordination shells. Then, the configuration-dependent contribution to the Gibbs free energy of such a solid solution (in the absence of external stresses on its surfaces) can be written as follows:

$$\begin{aligned} G \cong G_0 &+ \sum_{\alpha=\mathrm{N}_s,\upsilon}\sum_{\mathbf{R}} R^{\alpha}(\mathbf{R})P^{\alpha}(\mathbf{R}) + \sum_{\beta=\mathrm{N}_i,\varnothing}\sum_{p=1}^{3}\sum_{\mathbf{R}} R_p^{\beta}(\mathbf{R})P_p^{\beta}(\mathbf{R}) + \\ &+\frac{1}{2}\sum_{\alpha=\mathrm{Fe},\mathrm{N}_s,\upsilon}\ \sum_{\beta=\mathrm{Fe},\mathrm{N}_s,\upsilon}\ \sum_{\mathbf{R},\mathbf{R}'} W^{\alpha\beta}(\mathbf{R}-\mathbf{R}')P^{\alpha}(\mathbf{R})P^{\beta}(\mathbf{R}') + \\ &+\frac{1}{2}\sum_{\alpha=\mathrm{N}_i,\varnothing}\ \sum_{\beta=\mathrm{N}_i,\varnothing}\ \sum_{p,p'=1}^{3}\sum_{\mathbf{R},\mathbf{R}'} W_{pp'}^{\alpha\beta}(\mathbf{R}-\mathbf{R}')P_p^{\alpha}(\mathbf{R})P_{p'}^{\beta}(\mathbf{R}') + \\ &+\sum_{\alpha=\mathrm{Fe},\mathrm{N}_s,\upsilon}\ \sum_{\beta=\mathrm{N}_i,\varnothing}\ \sum_{p=1}^{3}\sum_{\mathbf{R},\mathbf{R}'} W_p^{\alpha\beta}(\mathbf{R}-\mathbf{R}')P^{\alpha}(\mathbf{R})P_p^{\beta}(\mathbf{R}') + \\ &+k_BT\sum_{\alpha=\mathrm{Fe},\mathrm{N}_s,\upsilon}\sum_{\mathbf{R}} P^{\alpha}(\mathbf{R})\ln P^{\alpha}(\mathbf{R}) + k_BT\sum_{\beta=\mathrm{N}_i,\varnothing}\sum_{p=1}^{3}\sum_{\mathbf{R}} P_p^{\beta}(\mathbf{R})\ln P_p^{\beta}(\mathbf{R}). \end{aligned} \tag{1}$$

Here, k_B is the Boltzmann constant; T is the absolute temperature of the solution; G_0 $\forall T$ is the Gibbs free energy part insensitive to configurations of all atoms; $R^\alpha(\mathbf{R}) \cong \text{const} = R^\alpha$ and $R^\alpha_p(\mathbf{R}) \cong \text{const} = R^\alpha_p = R^\alpha_1 = R^\alpha_2 = R^\alpha_3$ are the specific (per atom α) energies related to the 'expansion' or 'compression' of each of N_α atoms uniformly introduced into the sites and/or crystallographically-equivalent octahedral interstices of the b.c.c.(t.) Fe crystal [89, 91, 92, 98, 99]; $W^{\alpha\beta}(\mathbf{R} - \mathbf{R}')$, $W^{\alpha\beta}_{pp'}(\mathbf{R} - \mathbf{R}')$, or $W^{\alpha\beta}_p(\mathbf{R} - \mathbf{R}')$ are the effective pair interaction energies for the α and β atoms occupying sites with radius-vectors $\mathbf{R}$ and $\mathbf{R}'$, interstices with radius-vectors $\mathbf{R} + \mathbf{h}_p$ and $\mathbf{R}' + \mathbf{h}_{p'}$, or site $\mathbf{R}$ and interstice $\mathbf{R}' + \mathbf{h}_{p'}$, respectively.

The values of $P^{\mathrm{N}_i}_p(\mathbf{R})$ and $P^{\mathrm{N}_s}(\mathbf{R})$ relate to each other through the conservation condition for the total number of N atoms in interstices and sites ($N_\mathrm{N} = N_{\mathrm{N}_i} + N_{\mathrm{N}_s}$) during their redistribution:

$$N_\mathrm{N} = N_s(3\kappa_{\mathrm{N}_i} + \kappa_{\mathrm{N}_s}) = \sum_{\mathbf{R}}\left(\sum_{p=1}^{3} P^{\mathrm{N}_i}_p(\mathbf{R}) + P^{\mathrm{N}_s}(\mathbf{R})\right), \tag{2}$$

where, by definition for the relative concentrations $\kappa_{\mathrm{N}_i} = N_{\mathrm{N}_i}/(3N_s)$ and $\kappa_{\mathrm{N}_s} = N_{\mathrm{N}_s}/N_s$. Here and further, N_N (italic) denote total number of nitrogen atoms (and N_s is total number of sites), while N (regular) denotes chemical element 'nitrogen' (and N_s or N_i are nitrogen atoms in site and interstice, respectively). In addition, it is evidently that any site (interstice) in any of N_s primitive unit cells of the solvent has to be obligatory occupied by atoms of any allowable kind:

$$\forall\mathbf{R} \sum_{\alpha=\mathrm{Fe},\mathrm{N}_s,\upsilon} P^\alpha(\mathbf{R}) = 1, \tag{3}$$

and

$$\forall\mathbf{R} \sum_{\beta=\mathrm{N}_i,\varnothing} P^\beta_p(\mathbf{R}) = 1, \text{ where } p = 1, 2, 3. \tag{4}$$

Probabilities for interstices to be occupied by interstitial atoms N_i can be presented as the linear superpositions of the static concentration waves [92]:

$$P^{\mathrm{N}_i}_p(\mathbf{R}) = \overline{P}^{\mathrm{N}_i}_p(\mathbf{R}) + \delta P^{\mathrm{N}_i}_p(\mathbf{R}) = \overline{P}^{\mathrm{N}_i}_p + \sum_\tau\sum_{j_\tau}\delta\tilde{P}^{\mathrm{N}_i}_p(\mathbf{k}_{j_\tau})e^{i\mathbf{k}_{j_\tau}\cdot\mathbf{R}}.$$

Here,

$$\overline{P}^{\mathrm{N}_i}_p = \frac{1}{N_s}\sum_{\mathbf{R}} P^{\mathrm{N}_i}_p(\mathbf{R})$$

is the relative concentration of N_i atoms in the p-th interstitial sublattice of two-component interstitial subsystem N_i–∅. The amplitude of the plane wave $\exp(i\mathbf{k}_{j_\tau}\cdot\mathbf{R})$ can be represented as

$$\delta\tilde{P}^{\mathrm{N}_i}_p(\mathbf{k}_{j_\tau}) = \sum_{\omega=1}^{3}\eta^{\mathrm{N}_i}_{\omega\tau}\gamma^{\mathrm{N}_i}_{\omega\tau}(\mathbf{k}_{j_\tau})\psi_{\omega p}(\mathbf{k}_{j_\tau}).$$

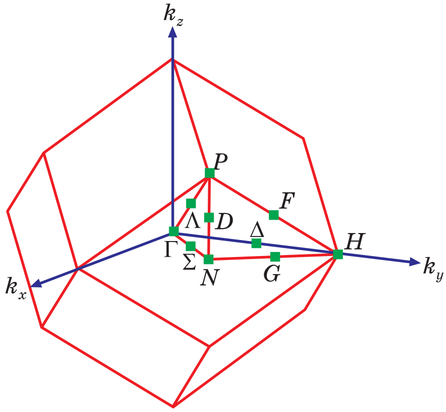

Fig. 5. The first Brillouin zone (*BZ*) of b.c.c. crystal. The Γ point ($\mathbf{k} = \mathbf{0}$) lies at the centre of the Brillouin zone. Here, we applied the standard designations to specify the symmetry points on the Brillouin zone boundary (*H*, *N*, *P*) and the symmetry axes within the Brillouin zone (Δ, Σ, Λ, *F*, *G*, *D*)

The symmetry coefficients $\{\gamma^{\mathrm{N}_i}_{\omega\tau}(\mathbf{k}_{j_\tau})\}$ are constant within the T–κ_{N_i}-range of thermodynamically stable existence of the phase. A set of these coefficients should be determined such that all linearly independent (non-negative by the definition) long-range order parameters $\{\eta^{\mathrm{N}_i}_{\omega\tau}\}$ equal to 1 for totally ordered solution of N_i within the b.c.c.(t.) Fe. Such a superstructural state means a single-phase of solid solution of stoichiometric composition ($\kappa_{\mathrm{N}_i} = \kappa^{\mathrm{st}}_{\mathrm{N}_i}$) described by the probabilities $\{P^{\mathrm{N}_i}_p(\mathbf{R})\}$ possessing only two values, 0 or 1, and can be realized only at a zero temperature (0 K). $\psi_{\omega p}(\mathbf{k}_{j_\tau})$ is the p-th component of the ω-th orthonormalized column vector of 'polarisation' of the static concentration wave $\psi_{\omega p}(\mathbf{k}_{j_\tau})\exp(i\mathbf{k}_{j_\tau}\cdot\mathbf{R})$ ($\omega = 1, 2, 3$). In such an expansion of $\delta P^{\mathrm{N}_i}_p(\mathbf{R})$, there exist only static concentration waves for those 'stars' τ of non-zero ($\tau \neq \Gamma$; see Fig. 5) wave vectors $\{\mathbf{k}^\tau\}$ (namely, rays $\{\mathbf{k}_{j_\tau}\}$ of the 'star' τ) with non-zero factors $\{\gamma^{\mathrm{N}_i}_{\omega\tau}(\mathbf{k}_{j_\tau})\}$ associated with atomic ordering.

Henceforth, we shall consider non-stoichiometric b.c.t.-Fe–N solid solution.

Suppose an ordered distribution of N_i atoms over the octahedral interstices [16, 17, 27, 28]. Then, for the α″-Fe$_{16}$N$_2$-type superstructure, the second terms in the occupation probabilities (amplitudes of the plane waves) can be represented as follow (see Ref. [100]):

$$\delta P^{\mathrm{N}_i}_1(\mathbf{R}) = \frac{1}{24}\left(\eta^{\mathrm{N}_i}_{2H} - \eta^{\mathrm{N}_i}_{1H}\right)e^{i\mathbf{k}_{1_H}\cdot\mathbf{R}} + \frac{1}{16}\left(\eta^{\mathrm{N}_i}_{1N} - \eta^{\mathrm{N}_i}_{2N}\right)\left(e^{i\mathbf{k}_{3_N}\cdot\mathbf{R}} + e^{i\mathbf{k}_{4_N}\cdot\mathbf{R}}\right), \tag{5a}$$

$$\delta P^{\mathrm{N}_i}_2(\mathbf{R}) = \frac{1}{24}\left(\eta^{\mathrm{N}_i}_{2H} - \eta^{\mathrm{N}_i}_{1H}\right)e^{i\mathbf{k}_{1_H}\cdot\mathbf{R}} + \frac{1}{16}\left(\eta^{\mathrm{N}_i}_{1N} - \eta^{\mathrm{N}_i}_{2N}\right)\left(e^{i\mathbf{k}_{5_N}\cdot\mathbf{R}} + e^{i\mathbf{k}_{6_N}\cdot\mathbf{R}}\right), \tag{5b}$$

$$\delta P^{\mathrm{N}_i}_3(\mathbf{R}) = \frac{1}{24}\left(2\eta^{\mathrm{N}_i}_{1H} + \eta^{\mathrm{N}_i}_{2H}\right)e^{i\mathbf{k}_{1_H}\cdot\mathbf{R}} + \frac{1}{8}\eta^{\mathrm{N}_i}_{3N}\left(e^{i\mathbf{k}_{1_N}\cdot\mathbf{R}} + e^{i\mathbf{k}_{2_N}\cdot\mathbf{R}}\right) +$$

$$+ \frac{1}{16}\left(\eta^{\mathrm{N}_i}_{1N} + \eta^{\mathrm{N}_i}_{2N}\right)\left(e^{i\mathbf{k}_{3_N}\cdot\mathbf{R}} + e^{i\mathbf{k}_{4_N}\cdot\mathbf{R}} + e^{i\mathbf{k}_{5_N}\cdot\mathbf{R}} + e^{i\mathbf{k}_{6_N}\cdot\mathbf{R}}\right), \tag{5c}$$

where (in the rectangular (Cartesian) coordinate system $Ok_xk_yk_z$) $\mathbf{k}_{1_H}$ is the vector of single-ray 'star' $\{\mathbf{k}^H\}$, and $\mathbf{k}_{1_N}$, $\mathbf{k}_{2_N}$, $\mathbf{k}_{3_N}$, $\mathbf{k}_{4_N}$, $\mathbf{k}_{5_N}$, $\mathbf{k}_{6_N}$ are vectors of six-rays' 'star' $\{\mathbf{k}^N\}$ (see Fig. 5):

$$\mathbf{k}_{1_H} = \frac{2\pi}{a_0}(0;1;0),$$

$$\mathbf{k}_{1_N} = \frac{2\pi}{a_0}\left(\frac{1}{2};\frac{1}{2};0\right),\ \mathbf{k}_{2_N} = \frac{2\pi}{a_0}\left(-\frac{1}{2};\frac{1}{2};0\right),\ \mathbf{k}_{3_N} = \frac{2\pi}{a_0}\left(\frac{1}{2};0;\frac{1}{2}\right),$$

$$\mathbf{k}_{4_N} = \frac{2\pi}{a_0}\left(-\frac{1}{2};0;\frac{1}{2}\right),\ \mathbf{k}_{5_N} = \frac{2\pi}{a_0}\left(0;\frac{1}{2};\frac{1}{2}\right),\ \mathbf{k}_{6_N} = \frac{2\pi}{a_0}\left(0;-\frac{1}{2};\frac{1}{2}\right).$$

Then, for virtually maximally ordered interstitial subsystem over the entire $T-\kappa_{\mathrm{N}_i}$ range of the existence of non-stoichiometric b.c.t.-Fe–N solid solution, the following relations should be satisfied:

$$\forall\mathbf{R}\ \ P_1^{\mathrm{N}_i}(\mathbf{R}) \cong 0,\ \ P_2^{\mathrm{N}_i}(\mathbf{R}) \cong 0,\ \ P_3^{\mathrm{N}_i}(\mathbf{R}) \cong 3\kappa_{\mathrm{N}_i}\left(1 + e^{i\mathbf{k}_{1_H}\cdot\mathbf{R}} + \sum_{j_N=1}^{6} e^{i\mathbf{k}_{j_N}\cdot\mathbf{R}}\right). \quad (6)$$

Let us assume that the translational symmetry of N_s atoms' distribution over the available (vacant) b.c.c.(t.) lattice sites coincides with the symmetry of N_i atoms' distribution in the preferable (3-rd in Fig. 2, bottom right) interstitial sublattice, however with the mutual arrangement of the firsts with respect to the latter so that the nearest neighbourhoods N_s–N_i are absent. The case of the nearest-neighbouring N_s–N_i atoms is excluded in order to be in accordance with strong ('blocking'), but short-range 'direct' ('contact'), '(electro)chemical' interatomic interaction N–N (see, *e.g.*, [98, 99]). The occupation-probability function described such an ordered distribution of N_s atoms over the (single) sublattice of sites,

$$P^{\mathrm{N}_s}(\mathbf{R}) = \kappa_{\mathrm{N}_s} - \frac{1}{8}\eta_H^{\mathrm{N}_s} e^{i\mathbf{k}_{1_H}\cdot\mathbf{R}} + \frac{1}{8}\eta_N^{\mathrm{N}_s}\sum_{j_N=1}^{6}(-1)^{j_N} e^{i\mathbf{k}_{j_N}\cdot\mathbf{R}}, \quad (7)$$

for the state with maximal long-range atomic order at the sites, which is possible at a fixed occupancy degree (relative concentration) κ_{N_s}, will have the following form:

$$P^{\mathrm{N}_s}(\mathbf{R}) \cong \kappa_{\mathrm{N}_s}\left(1 - e^{i\mathbf{k}_{1_H}\cdot\mathbf{R}} + \sum_{j_N=1}^{6}(-1)^{j_N} e^{i\mathbf{k}_{j_N}\cdot\mathbf{R}}\right). \quad (8)$$

In addition, we assume that the sites υ, which remained unoccupied by substituting atoms of Fe and N, are distributed 'in disordered manner' over the b.c.c.(t.) lattice in the sense that $P^{\upsilon}(\mathbf{R}) \cong \kappa_{\upsilon} = \mathrm{N}_{\upsilon}/\mathrm{N}_s$, where N_{υ} is the number of such (residual) monovacancies. Here, we assume that, practically, there are no mixed υ–N_i complexes [101], υ–N_s neighbourhoods, complexions of N atoms at the sites, and the number of these defects is small as compared to the number of lattice sites.

The long-range order of Fe and N_s atoms over the sites, when they 'repeat' the ordered interstitial N_i and ∅ 'atoms' within the confines of only the third sublattice of octahedral interstices (as for α″-F$_{16}$N$_2$ phase), can be attributed to 'repulsive' N_i–Fe and N_i–N_i interactions between the interstitial and substitutional subsystems, rather than 'attractive' (Fe–Fe) and 'repulsive' (Fe–N_s, N_s–N_s) interactions in the substitutional Fe–N_s subsystem. Then, taking into account Eq. (1), relations (3), (4), and assuming relations (6) and (8), one can easy to obtain the expression of specific (*i.e.*, with respect to the total number N_{Fe} of Fe ions) Gibbs free energy g for such an 'ordered' phase of the b.c.t.-Fe–N solution at zero external pressure:

$$
\begin{aligned}
g \cong{}& g_{\varnothing} + R^{\mathrm{N}_s}c_{\mathrm{N}_s} + R^{v}c_{v} + R_3^{\mathrm{N}_i}c_{\mathrm{N}_i} + \\
&+(1+c_{\mathrm{N}_s}+c_v)^{-1}\left\{\frac{1}{2}\tilde{W}^{\mathrm{FeFe}}(\mathbf{0}) + \tilde{W}^{\mathrm{FeN}_s}(\mathbf{0})c_{\mathrm{N}_s} + \tilde{W}^{\mathrm{Fe}v}(\mathbf{0})c_v + \right.\\
&+\tilde{W}_3^{\mathrm{FeN}_i}(\mathbf{0})c_{\mathrm{N}_i} + \tilde{W}^{\mathrm{N}_s v}(\mathbf{0})c_{\mathrm{N}_s}c_v + \tilde{W}_3^{v\mathrm{N}_i}(\mathbf{0})c_{\mathrm{N}_i}c_v + \\
&+\left[\tilde{W}_3^{\mathrm{N}_s\mathrm{N}_i}(\mathbf{0}) - \tilde{W}_3^{\mathrm{N}_s\mathrm{N}_i}(\mathbf{k}_{1_H}) + \tilde{W}_3^{\mathrm{FeN}_i}(\mathbf{k}_{1_H}) + \right.\\
&\left.+\sum_{j_N=1}^{6}(-1)^{j_N}\left(\tilde{W}_3^{\mathrm{N}_s\mathrm{N}_i}(\mathbf{k}_{j_N}) - \tilde{W}_3^{\mathrm{FeN}_i}(\mathbf{k}_{j_N})\right)\right]c_{\mathrm{N}_i}c_{\mathrm{N}_s} + \\
&+\frac{1}{2}\left(\tilde{W}^{\mathrm{N}_s\mathrm{N}_s}(\mathbf{0}) + \tilde{w}^{\mathrm{FeN}_s}(\mathbf{k}_{1_H}) + 6\tilde{w}^{\mathrm{FeN}_s}(\mathbf{k}_{1_N})\right)c_{\mathrm{N}_s}^2 + \frac{1}{2}\tilde{W}^{vv}(\mathbf{0})c_v^2 + \\
&\left.+\frac{1}{2}\left(\tilde{W}_{33}^{\mathrm{N}_i\mathrm{N}_i}(\mathbf{0}) + \tilde{W}_{33}^{\mathrm{N}_i\mathrm{N}_i}(\mathbf{k}_{1_H}) + 4\tilde{W}_{11}^{\mathrm{N}_i\mathrm{N}_i}(\mathbf{k}_{1_N}) + 2\tilde{W}_{33}^{\mathrm{N}_i\mathrm{N}_i}(\mathbf{k}_{1_N})\right)c_{\mathrm{N}_i}^2\right\} + \\
&+\frac{k_BT}{8}\Big\{7(1+c_{\mathrm{N}_s})\ln(1+c_{\mathrm{N}_s}) + (1-7c_{\mathrm{N}_s})\ln(1-7c_{\mathrm{N}_s}) + \\
&+8c_{\mathrm{N}_s}\ln(8c_{\mathrm{N}_s}) + 8c_v\ln(8c_v) + 8c_{\mathrm{N}_i}\ln(8c_{\mathrm{N}_i}) + \\
&+(1+c_{\mathrm{N}_s}+c_v-8c_{\mathrm{N}_i})\ln(1+c_{\mathrm{N}_s}+c_v-8c_{\mathrm{N}_i}) - \\
&-9(1+c_{\mathrm{N}_s}+c_v)\ln(1+c_{\mathrm{N}_s}+c_v)\Big\},
\end{aligned}
\tag{9}
$$

where $g_{\varnothing}$ is non-configurational part of g, $\tilde{W}^{\alpha\beta}(\mathbf{k})$, $\tilde{W}_{pp}^{\mathrm{N}_i\mathrm{N}_i}(\mathbf{k})$ and $\tilde{W}_p^{\alpha\mathrm{N}_i}(\mathbf{k})$ are $\mathbf{k}$-th ($\mathbf{k}=\mathbf{0}$, $\mathbf{k}=\mathbf{k}_{1_H}$, $\mathbf{k}=\mathbf{k}_{j_N}$) Fourier components of the effective pair interaction energies of atoms of corresponding constituents in the b.c.t.-Fe–N solution, $\tilde{w}^{\mathrm{FeN}_s}(\mathbf{k}_{1_H})$ and $\tilde{w}^{\mathrm{FeN}_s}(\mathbf{k}_{1_N})$ are the Fourier components (in the $\mathbf{k}_{1_H}$ and $\mathbf{k}_{1_N}$ points of the 1-st Brillouin zone of b.c.c. Fe) of 'mixing' ('interchange') energies

$$w^{\mathrm{FeN}_s}(\mathbf{R}-\mathbf{R}') = W^{\mathrm{FeFe}}(\mathbf{R}-\mathbf{R}') + W^{\mathrm{N}_s\mathrm{N}_s}(\mathbf{R}-\mathbf{R}') - 2W^{\mathrm{FeN}_s}(\mathbf{R}-\mathbf{R}').$$

The values

$$c_v = \frac{N_v}{N_{\text{Fe}}},\ c_{\text{N}_i} = \frac{N_{\text{N}_i}}{N_{\text{Fe}}},\ c_{\text{N}_s} = \frac{N_{\text{N}_s}}{N_{\text{Fe}}}$$

denote the 'relative' concentrations of the residual vacancies v, and N atoms intruded into octahedral interstices and occupying the (smaller) part of sites in b.c.t. Fe, respectively. According to Eq. (2),

$$c_{\text{N}_i} + c_{\text{N}_s} = c_{\text{N}} = \frac{N_{\text{N}}}{N_{\text{Fe}}}.$$

We have to note that, in Eq. (9), the contributions of 'soft' (Coulomb-type) α–$\varnothing$ interactions were omitted as negligibly small. The magnetic contribution (mainly, due to the exchange interaction of Fe atoms) is implicitly contained in the 'mixing' energies (*e.g.*, see explicit expressions for the exchange Fe–Fe-interaction integrals in Ref. [102]), if temperature T is below the Curie point $T_C = T_C(c_{\text{N}_i}, c_{\text{N}_s} + c_v)$.

Note also that, in fifth summand in right side of Eq. (1), the summation is carried out over all **(!)** interstices $\{p, \mathbf{R}\}$ and $\{p', \mathbf{R}'\}$ of the host Bravais lattice. So, statistical thermodynamics of interstitial atomic ordering in the case of three octahedral-interstices' sublattices in the b.c.c. host lattice is described with elements of the $\|\tilde{W}_{p\,p'}^{\text{N}_i\text{N}_i}(\mathbf{k})\|$ matrix of Fourier transforms (see Eq. (9)), which has the form

$$\begin{pmatrix} \tilde{W}_{1\,1}^{\text{N}_i\text{N}_i}(\mathbf{k}) & \tilde{W}_{1\,2}^{\text{N}_i\text{N}_i}(\mathbf{k}) & \tilde{W}_{1\,3}^{\text{N}_i\text{N}_i}(\mathbf{k}) \\ \left[\tilde{W}_{1\,2}^{\text{N}_i\text{N}_i}(\mathbf{k})\right]^* & \tilde{W}_{2\,2}^{\text{N}_i\text{N}_i}(\mathbf{k}) & \tilde{W}_{2\,3}^{\text{N}_i\text{N}_i}(\mathbf{k}) \\ \left[\tilde{W}_{1\,3}^{\text{N}_i\text{N}_i}(\mathbf{k})\right]^* & \left[\tilde{W}_{2\,3}^{\text{N}_i\text{N}_i}(\mathbf{k})\right]^* & \tilde{W}_{3\,3}^{\text{N}_i\text{N}_i}(\mathbf{k}) \end{pmatrix},$$

where, according to both the equality $W_{p\,p'}^{\text{N}_i\text{N}_i}(\mathbf{R}-\mathbf{R}') = W_{p'\,p}^{\text{N}_i\text{N}_i}(\mathbf{R}'-\mathbf{R})$ and the definition of Fourier transformation, the Hermitian character of above-mentioned 'interaction' matrix $\|\tilde{W}_{p\,p'}^{\text{N}_i\text{N}_i}(\mathbf{k})\|$ is utilized:

$$\tilde{W}_{2\,1}^{\text{N}_i\text{N}_i}(\mathbf{k}) = \left[\tilde{W}_{1\,2}^{\text{N}_i\text{N}_i}(\mathbf{k})\right]^* \text{ and } \tilde{W}_{3\,2}^{\text{N}_i\text{N}_i}(\mathbf{k}) = \left[\tilde{W}_{2\,3}^{\text{N}_i\text{N}_i}(\mathbf{k})\right]^*.$$

The elements of the $\|\tilde{W}_{p\,p'}^{\text{N}_i\text{N}_i}(\mathbf{k})\|$ matrix may easily be calculated within the framework of the *short-range* interatomic-interaction approximation. For instance, if and only if,

$$\forall \mathbf{k} \in BZ\ \tilde{W}_{3\,3}^{\text{N}_i\text{N}_i}(\mathbf{k}) = \tilde{W}_{1\,1}^{\text{N}_i\text{N}_i}(\mathbf{k}) = \tilde{W}_{2\,2}^{\text{N}_i\text{N}_i}(\mathbf{k}).$$

Nevertheless, even if the interatomic interactions are *long-ranging*, by symmetry, for $\mathbf{k} = \mathbf{0}$, the matrix $\|\tilde{W}_{p\,p'}^{\text{N}_i\text{N}_i}(\mathbf{0})\|$ always has the form [92]

$$\begin{pmatrix} \tilde{W}^{\mathrm{N}_i\mathrm{N}_i}_{3\,3}(\mathbf{0}) & \tilde{W}^{\mathrm{N}_i\mathrm{N}_i}_{1\,2}(\mathbf{0}) & \tilde{W}^{\mathrm{N}_i\mathrm{N}_i}_{1\,2}(\mathbf{0}) \\ \tilde{W}^{\mathrm{N}_i\mathrm{N}_i}_{1\,2}(\mathbf{0}) & \tilde{W}^{\mathrm{N}_i\mathrm{N}_i}_{3\,3}(\mathbf{0}) & \tilde{W}^{\mathrm{N}_i\mathrm{N}_i}_{1\,2}(\mathbf{0}) \\ \tilde{W}^{\mathrm{N}_i\mathrm{N}_i}_{1\,2}(\mathbf{0}) & \tilde{W}^{\mathrm{N}_i\mathrm{N}_i}_{1\,2}(\mathbf{0}) & \tilde{W}^{\mathrm{N}_i\mathrm{N}_i}_{3\,3}(\mathbf{0}) \end{pmatrix}.$$

Moreover, the symmetry considerations applied to the matrix $\|\tilde{W}^{\mathrm{N}_i\mathrm{N}_i}_{p\,p'}(\mathbf{k}_{j_N})\|$ always result in the form [92]

$$\begin{pmatrix} \tilde{W}^{\mathrm{N}_i\mathrm{N}_i}_{1\,1}(\mathbf{k}_{j_N}) & \tilde{W}^{\mathrm{N}_i\mathrm{N}_i}_{1\,2}(\mathbf{k}_{j_N}) & 0 \\ \tilde{W}^{\mathrm{N}_i\mathrm{N}_i}_{1\,2}(\mathbf{k}_{j_N}) & \tilde{W}^{\mathrm{N}_i\mathrm{N}_i}_{1\,1}(\mathbf{k}_{j_N}) & 0 \\ 0 & 0 & \tilde{W}^{\mathrm{N}_i\mathrm{N}_i}_{3\,3}(\mathbf{k}_{j_N}) \end{pmatrix},$$

where $\{\mathbf{k}_{j_N}\}$ are the vectors of six-rays' 'star' of quasi-wave vector $\mathbf{k}^N$ corresponding to high-symmetry point N of the BZ edge (see Fig. 5).

In conclusion of this subsection note that the possibility of strong interatomic interactions up to the appearance of the 'blocking' effect (at least for small distances), when, *e.g.*, $|w^{\mathrm{FeN}_s}(\mathbf{R}-\mathbf{R}')| \gg k_BT$ and/or $|\tilde{W}^{\mathrm{N}_i\mathrm{N}_i}_{p\,p}(\mathbf{R}-\mathbf{R}')| \gg k_BT$ for $|\mathbf{R}-\mathbf{R}'| = o^*(a_0)$, assumes a consistent accounting the correlation effects, when we calculate thermodynamic properties in the equilibrium state. In this case, one has to expect that the self-consistent mean field approximation, which does not take into account the short- and long-range correlations in the mutual atomic spatial distributions, is unreasonable. This inapplicability deals, first of all, with the substitutional subsystem, where the equilibrium coordination ('radial' + 'angular') long-range atomic order appears no faster than the short-range ('angular') order. In essence, the long-range order appears due to the development of the noticeable equilibrium correlations in both the arrangements of different types of ions (in more and more distant coordination shells) and the orientations of 'bonds' between them. This process tends to be realized, in particular, thorough over-barrier diffusion mechanisms of interchange of Fe- and N_s-atomic locations and/or through the migration of atoms N_s, Fe, and v by means of a large number of elementary jumps to the relevant distances. These distances should be comparable with characteristic length, ξ_{0s}, of the spatial correlation of large-scale fluctuations of atomic order or with (related to ξ_{0s}) spatial scale parameter [91]

$$\mathfrak{R}_s \cong \sqrt{\frac{\sum_{\mathbf{R}'}|\mathbf{R}-\mathbf{R}'|^2 K^{\mathrm{N}_s\mathrm{N}_s}(\mathbf{R}-\mathbf{R}')}{\sum_{\mathbf{R}'} K^{\mathrm{N}_s\mathrm{N}_s}(\mathbf{R}-\mathbf{R}')}},$$

which is typical geometric dimension of the 'domain' with developed order or, in a general way, the continuity region of any topological feature of a homogeneous random field $\{c^{\mathrm{N}_s}(\mathbf{R})\}$, whether its 'peak' (1) or 'valley' (0) are the characteristics of N_s-atomic distribution over the sites. The correlation function

$$K^{N_sN_s}(\mathbf{R}-\mathbf{R}') = \left\langle \{c^{N_s}(\mathbf{R}) - \kappa_{N_s}\}\,\{c^{N_s}(\mathbf{R}') - \kappa_{N_s}\}\right\rangle$$

is normalized to 1 for $\mathbf{R}' = \mathbf{R}$ and tends monotonically to zero with increasing interatomic distance $r = |\mathbf{R}-\mathbf{R}'|$; however, even for large $r(\gg a_0)$ $K^{N_sN_s}(\mathbf{R}-\mathbf{R}') \propto r^{-1}e^{-r/\xi_{0s}}$ [103]). Therefore, for T in a vicinity above the 'critical' temperature T_{0s} (conventionally, 'for the substitutional subsystem') determined in the self-consistent mean-field approximation (with account of the 'action' of the effective interstitial-subsystem-induced external field), where $\xi_{0s} \propto a_0\sqrt{T_{0s}/|T_{0s}-T|}$ [103], the stable equilibrium-order state in the substitutional subsystem is realized only after the passage of a comparatively long interval of time $\tau \propto \xi_{0s}^2/\tilde{D}$ ($>\Re_s^2/\tilde{D}$, where $\tilde{D}$ is the interdiffusion coefficient) and also includes the establishment of equilibrium spatial correlations [92]. Note that statistically equilibrium 'orientational' long-range order is attained in the interstitial subsystem already at the early relaxation stage by means of the only elementary diffusion act that is the N_i-atomic jumps into the nearest-neighbour unoccupied interstices [92], *i.e.*, it occurs considerably faster than noticeable equilibrium correlation effects. Nevertheless, the mentioned issue can be circumvented if one notes a certain circumstance associate with the specific character of the proposed structural state, namely, with the maximum ordering of both solution subsystems (under the conditions of even relative equilibrium): in this state, correlation effects are insignificant [103]. This fact provides the asymptotic accuracy of the self-consistent mean-field approximation [92] applied to describe the thermodynamic characteristics interesting us.

3. Tetragonality of Fe–N Martensite under the Conditions of a Dynamic Statistical Equilibrium

Thermodynamically equilibrium values of two independent variables c_v and c_{N_i} can be obtained from the set of equations:

$$\begin{aligned}
&-R^{v} - \frac{1}{2}\tilde{W}^{vv}(\mathbf{0}) + (1 + c_{N_s} + c_v)^{-2}\left\{\frac{1}{2}\tilde{w}^{\mathrm{Fe}v}(\mathbf{0}) +\right.\\
&+\left(\tilde{W}^{\mathrm{Fe}N_s}(\mathbf{0}) + \tilde{W}^{vv}(\mathbf{0}) - \tilde{W}^{N_sv}(\mathbf{0}) - \tilde{W}^{\mathrm{Fe}v}(\mathbf{0})\right)c_{N_s} +\\
&+\left(\tilde{W}_3^{\mathrm{Fe}N_i}(\mathbf{0}) - \tilde{W}_3^{vN_i}(\mathbf{0})\right)c_{N_i} +\\
&+\left[\tilde{W}_3^{N_sN_i}(\mathbf{0}) - \tilde{W}_3^{vN_i}(\mathbf{0})c_{N_i} - \tilde{W}_3^{N_sN_i}(\mathbf{k}_{1_H}) + \tilde{W}_3^{\mathrm{Fe}N_i}(\mathbf{k}_{1_H}) +\right.\\
&\left.+\sum_{j_N=1}^{6}(-1)^{j_N}\left(\tilde{W}_3^{N_sN_i}(\mathbf{k}_{j_N}) - \tilde{W}_3^{\mathrm{Fe}N_i}(\mathbf{k}_{j_N})\right)\right]c_{N_s}c_{N_i} +
\end{aligned}$$

$$+\frac{1}{2}\Big(\tilde{w}^{\mathrm{N}_s v}(\mathbf{0})+\tilde{w}^{\mathrm{FeN}_s}(\mathbf{k}_{1_H})+6\tilde{w}^{\mathrm{FeN}_s}(\mathbf{k}_{1_N})\Big)c_{\mathrm{N}_s}^2+$$

$$+\frac{1}{2}\Big(\tilde{W}^{\mathrm{N}_i\mathrm{N}_i}_{\;3\;3}(\mathbf{0})+\tilde{W}^{\mathrm{N}_i\mathrm{N}_i}_{\;3\;3}(\mathbf{k}_{1_H})+4\tilde{W}^{\mathrm{N}_i\mathrm{N}_i}_{\;1\;1}(\mathbf{k}_{1_N})+2\tilde{W}^{\mathrm{N}_i\mathrm{N}_i}_{\;3\;3}(\mathbf{k}_{1_N})\Big)c_{\mathrm{N}_i}^2\Bigg\}\approx$$

$$\approx k_BT\ln\left\{c_v\sqrt[8]{\frac{1+c_{\mathrm{N}_s}+c_v-8c_{\mathrm{N}_i}}{(1+c_{\mathrm{N}_s}+c_v)^9}}\right\}\qquad(10)$$

and

$$R^{\mathrm{N}_i}-R^{\mathrm{N}_s}-\frac{1}{2}\tilde{W}^{\mathrm{N}_s\mathrm{N}_s}(\mathbf{0})+(1+c_{\mathrm{N}_s}+c_v)^{-1}\Bigg\{\tilde{W}^{\mathrm{FeN}_i}_{\quad 3}(\mathbf{0})+$$

$$+\Bigg[\tilde{W}^{\mathrm{N}_s\mathrm{N}_i}_{\quad 3}(\mathbf{0})-\tilde{W}^{\mathrm{N}_s\mathrm{N}_i}_{\quad 3}(\mathbf{k}_{1_H})+\tilde{W}^{\mathrm{FeN}_i}_{\quad 3}(\mathbf{k}_{1_H})+$$

$$+\sum_{j_N=1}^{6}(-1)^{j_N}\Big(\tilde{W}^{\mathrm{N}_s\mathrm{N}_i}_{\quad 3}(\mathbf{k}_{j_N})-\tilde{W}^{\mathrm{FeN}_i}_{\quad 3}(\mathbf{k}_{j_N})\Big)\Bigg]c_{\mathrm{N}_s}+\tilde{W}^{v\mathrm{N}_i}_{\quad 3}(0)\,c_v+$$

$$+\Big(\tilde{W}^{\mathrm{N}_i\mathrm{N}_i}_{\;3\;3}(\mathbf{0})+\tilde{W}^{\mathrm{N}_i\mathrm{N}_i}_{\;3\;3}(\mathbf{k}_{1_H})+4\tilde{W}^{\mathrm{N}_i\mathrm{N}_i}_{\;1\;1}(\mathbf{k}_{1_N})+2\tilde{W}^{\mathrm{N}_i\mathrm{N}_i}_{\;3\;3}(\mathbf{k}_{1_N})\Big)c_{\mathrm{N}_i}\Bigg\}+$$

$$+(1+c_{\mathrm{N}_s}+c_v)^{-2}\Bigg\{\frac{1}{2}\tilde{w}^{\mathrm{FeN}_s}(\mathbf{0})+\Big(\tilde{W}^{\mathrm{Fe}v}(\mathbf{0})+\tilde{W}^{vv}(\mathbf{0})-\tilde{W}^{\mathrm{FeN}_s}(\mathbf{0})-\tilde{W}^{\mathrm{N}_s v}(\mathbf{0})\Big)c_v+$$

$$+\tilde{W}^{\mathrm{FeN}_i}_{\quad 3}(\mathbf{0})c_{\mathrm{N}_i}-\frac{1}{2}\Big(\tilde{w}^{\mathrm{FeN}_s}(\mathbf{k}_{1_H})+6\tilde{w}^{\mathrm{FeN}_s}(\mathbf{k}_{1_N})\Big)\Big(2c_{\mathrm{N}_s}(1+c_v)+c_{\mathrm{N}_s}^2\Big)-$$

$$-\Bigg[\tilde{W}^{\mathrm{N}_s\mathrm{N}_i}_{\quad 3}(\mathbf{0})-\tilde{W}^{\mathrm{N}_s\mathrm{N}_i}_{\quad 3}(\mathbf{k}_{1_H})+\tilde{W}^{\mathrm{FeN}_i}_{\quad 3}(\mathbf{k}_{1_H})+$$

$$+\sum_{j_N=1}^{6}(-1)^{j_N}\Big(\tilde{W}^{\mathrm{N}_s\mathrm{N}_i}_{\quad 3}(\mathbf{k}_{j_N})-\tilde{W}^{\mathrm{FeN}_i}_{\quad 3}(\mathbf{k}_{j_N})\Big)\Bigg]c_{\mathrm{N}_i}(1+c_v)+$$

$$+\tilde{W}^{v\mathrm{N}_i}_{\quad 3}(\mathbf{0})\,c_{\mathrm{N}_i}c_v+\frac{1}{2}\tilde{w}^{\mathrm{N}_s v}(\mathbf{0})c_v^2+$$

$$+\frac{1}{2}\Big(\tilde{W}^{\mathrm{N}_i\mathrm{N}_i}_{\;3\;3}(\mathbf{0})+\tilde{W}^{\mathrm{N}_i\mathrm{N}_i}_{\;3\;3}(\mathbf{k}_{1_H})+4\tilde{W}^{\mathrm{N}_i\mathrm{N}_i}_{\;1\;1}(\mathbf{k}_{1_N})+2\tilde{W}^{\mathrm{N}_i\mathrm{N}_i}_{\;3\;3}(\mathbf{k}_{1_N})\Big)c_{\mathrm{N}_i}^2\Bigg\}\approx$$

$$\approx k_BT\ln\left\{\frac{c_{\mathrm{N}_s}}{c_{\mathrm{N}_i}}\sqrt[8]{\frac{(1+c_{\mathrm{N}_s})^7(1+c_{\mathrm{N}_s}+c_v-8c_{\mathrm{N}_i})^9}{(1-7c_{\mathrm{N}_s})^7(1+c_{\mathrm{N}_s}+c_v)^9}}\right\},\qquad(11)$$

where

$$\tilde{w}^{\mathrm{Fe}v}(\mathbf{0})=\tilde{W}^{\mathrm{FeFe}}(\mathbf{0})+\tilde{W}^{vv}(\mathbf{0})-2\tilde{W}^{\mathrm{Fe}v}(\mathbf{0})\equiv\tilde{w}(\mathbf{0}),$$

$$\tilde{w}^{\mathrm{N}_s v}(\mathbf{0})=\tilde{W}^{\mathrm{N}_s\mathrm{N}_s}(\mathbf{0})+\tilde{W}^{vv}(\mathbf{0})-2\tilde{W}^{\mathrm{N}_s v}(\mathbf{0}),$$

$$\tilde{w}^{\mathrm{FeN}_s}(\mathbf{0})=\tilde{W}^{\mathrm{FeFe}}(\mathbf{0})+\tilde{W}^{\mathrm{N}_s\mathrm{N}_s}(\mathbf{0})-\tilde{W}^{\mathrm{FeN}_s}(\mathbf{0}).$$

In the first approximation, $0 < c_v \ll (1 + c_{\mathrm{N}_s} - 8c_{\mathrm{N}_i})$, and if in Eq. (11) we neglect the terms containing the factor c_v or, moreover, c_v^2, the set of coupled equations (10) and (11) reduces to two equations. The second one, Eq. (11), now does not contain c_v explicitly, and it serves to determine the equilibrium values of c_{N_i} and, consequently, $c_{\mathrm{N}_s} = c_{\mathrm{N}} - c_{\mathrm{N}_i}$ (for the given T and c_{N}):

$$\begin{aligned}
&R^{\mathrm{N}_i} - R^{\mathrm{N}_s} - \frac{1}{2}\tilde{W}^{\mathrm{N}_s\mathrm{N}_s}(\mathbf{0}) + (1 + c_{\mathrm{N}_s})^{-1}\Big\{\tilde{W}^{\mathrm{FeN}_i}_{3}(\mathbf{0}) + \\
&+\Big[\tilde{W}^{\mathrm{N}_s\mathrm{N}_i}_{3}(\mathbf{0}) - \tilde{W}^{\mathrm{N}_s\mathrm{N}_i}_{3}(\mathbf{k}_{1_H}) + \tilde{W}^{\mathrm{FeN}_i}_{3}(\mathbf{k}_{1_H}) + \\
&+\sum_{j_N=1}^{6}(-1)^{j_N}\Big(\tilde{W}^{\mathrm{N}_s\mathrm{N}_i}_{3}(\mathbf{k}_{j_N}) - \tilde{W}^{\mathrm{FeN}_i}_{3}(\mathbf{k}_{j_N})\Big)\Big]c_{\mathrm{N}_s} + \\
&+\Big(\tilde{W}^{\mathrm{N}_i\mathrm{N}_i}_{3\,3}(\mathbf{0}) + \tilde{W}^{\mathrm{N}_i\mathrm{N}_i}_{3\,3}(\mathbf{k}_{1_H}) + 4\tilde{W}^{\mathrm{N}_i\mathrm{N}_i}_{1\,1}(\mathbf{k}_{1_N}) + 2\tilde{W}^{\mathrm{N}_i\mathrm{N}_i}_{3\,3}(\mathbf{k}_{1_N})\Big)c_{\mathrm{N}_i}\Big\} + \\
&+(1 + c_{\mathrm{N}_s})^{-2}\Big\{\frac{1}{2}\tilde{w}^{\mathrm{FeN}_s}(\mathbf{0}) - \frac{1}{2}\Big(\tilde{w}^{\mathrm{FeN}_s}(\mathbf{k}_{1_H}) + 6\tilde{w}^{\mathrm{FeN}_s}(\mathbf{k}_{1_N})\Big)(2 + c_{\mathrm{N}_s})\,c_{\mathrm{N}_s} - \\
&-\Big[\tilde{W}^{\mathrm{N}_s\mathrm{N}_i}_{3}(\mathbf{0}) - \tilde{W}^{\mathrm{FeN}_i}_{3}(\mathbf{0}) - \tilde{W}^{\mathrm{N}_s\mathrm{N}_i}_{3}(\mathbf{k}_{1_H}) + \tilde{W}^{\mathrm{FeN}_i}_{3}(\mathbf{k}_{1_H}) + \\
&+\sum_{j_N=1}^{6}(-1)^{j_N}\Big(\tilde{W}^{\mathrm{N}_s\mathrm{N}_i}_{3}(\mathbf{k}_{j_N}) - \tilde{W}^{\mathrm{FeN}_i}_{3}(\mathbf{k}_{j_N})\Big)\Big]c_{\mathrm{N}_i} + \\
&+\frac{1}{2}\Big(\tilde{W}^{\mathrm{N}_i\mathrm{N}_i}_{3\,3}(\mathbf{0}) + \tilde{W}^{\mathrm{N}_i\mathrm{N}_i}_{3\,3}(\mathbf{k}_{1_H}) + 4\tilde{W}^{\mathrm{N}_i\mathrm{N}_i}_{1\,1}(\mathbf{k}_{1_N}) + 2\tilde{W}^{\mathrm{N}_i\mathrm{N}_i}_{3\,3}(\mathbf{k}_{1_N})\Big)c_{\mathrm{N}_i}^2\Big\} \cong \\
&\cong k_BT\ln\left\{\frac{c_{\mathrm{N}_s}}{c_{\mathrm{N}_i}}\sqrt[8]{\frac{(1 + c_{\mathrm{N}_s} - 8c_{\mathrm{N}_i})^9}{(1 - 7c_{\mathrm{N}_s})^7(1 + c_{\mathrm{N}_s})^2}}\right\}.
\end{aligned} \tag{12}$$

As for Eq. (10), it transforms simply into an expression for determining c_v for given $c_{\mathrm{N}_i}(T, c_{\mathrm{N}})$, $c_{\mathrm{N}_s}(T, c_{\mathrm{N}})$, and T):

$$\begin{aligned}
&c_v \cong c_v^{0'}\sqrt[8]{\frac{1 + c_{\mathrm{N}_s} - 8c_{\mathrm{N}_i}}{(1 + c_{\mathrm{N}_s})^9}}\exp\left(-\frac{2R^v + \tilde{W}^{vv}(\mathbf{0})}{2k_BT}\right)\times \\
&\times\exp\Bigg(\frac{1}{2k_BT}(1 + c_{\mathrm{N}_s})^{-2}\Big[2\Big(\tilde{W}^{\mathrm{FeN}_s}(\mathbf{0}) + \tilde{W}^{vv}(\mathbf{0}) - \tilde{W}^{\mathrm{N}_s v}(\mathbf{0}) - \tilde{W}^{\mathrm{Fe}v}(\mathbf{0})\Big)c_{\mathrm{N}_s} + \\
&+\Big(\tilde{W}^{\mathrm{FeN}_i}_{3}(\mathbf{0}) - \tilde{W}^{v\mathrm{N}_i}_{3}(\mathbf{0})\Big)c_{\mathrm{N}_i} + \\
&+\Big\{\tilde{W}^{\mathrm{N}_s\mathrm{N}_i}_{3}(\mathbf{0}) - \tilde{W}^{v\mathrm{N}_i}_{3}(\mathbf{0})c_{\mathrm{N}_i} - \tilde{W}^{\mathrm{N}_s\mathrm{N}_i}_{3}(\mathbf{k}_{1_H}) + \tilde{W}^{\mathrm{FeN}_i}_{3}(\mathbf{k}_{1_H}) +
\end{aligned}$$

$$+\sum_{j_N=1}^{6}(-1)^{j_N}\left(\tilde{W}^{\mathrm{N}_s\mathrm{N}_i}_{\ 3}(\mathbf{k}_{j_N})-\tilde{W}^{\mathrm{FeN}_i}_{\ \ 3}(\mathbf{k}_{j_N})\right)\Bigg\}c_{\mathrm{N}_s}c_{\mathrm{N}_i}+$$

$$+\frac{1}{2}\left(\tilde{w}^{\mathrm{N}_s v}(\mathbf{0})+\tilde{w}^{\mathrm{FeN}_s}(\mathbf{k}_{1_H})+6\tilde{w}^{\mathrm{FeN}_s}(\mathbf{k}_{1_N})\right)c^2_{\mathrm{N}_s}+$$

$$+\frac{1}{2}\left(\tilde{W}^{\mathrm{N}_i\mathrm{N}_i}_{3\,3}(\mathbf{0})+\tilde{W}^{\mathrm{N}_i\mathrm{N}_i}_{3\,3}(\mathbf{k}_{1_H})+4\tilde{W}^{\mathrm{N}_i\mathrm{N}_i}_{1\,1}(\mathbf{k}_{1_N})+2\tilde{W}^{\mathrm{N}_i\mathrm{N}_i}_{3\,3}(\mathbf{k}_{1_N})\right)c^2_{\mathrm{N}_i}\Bigg]\Bigg), \quad (13)$$

where the value

$$c_v^{0'}=\exp\left(-\frac{\tilde{w}^{\mathrm{Fe}v}(\mathbf{0})}{2k_BT(1+c_{\mathrm{N}_s})^2}\right)$$

equals to the 'relative' concentration c_v^0 ($\ll 1$) of thermally activated vacancies in the b.c.c. Fe only in the hypothetical case of $c_{\mathrm{N}_s}\equiv 0$.

The degree of tetragonality of a (weak) b.c.t.-Fe–N solution (isostructural to iron–nitrogen martensite) is determined by the ratio of the main geometrical parameters $a(c_\mathrm{N})$ and $b(c_\mathrm{N})$ of the conventional lattice cell. In its maximally ordered state, it is approximately proportional to the concentration of N atoms accumulated on only one of three sublattices of octahedral interstices [92, 96]:

$$\frac{b}{a}\cong 1+(L_3^{\mathrm{N}_i}-L_1^{\mathrm{N}_i})c_{\mathrm{N}_i}, \quad (14)$$

where

$$L_3^{\mathrm{N}_i}\equiv L_{3zz}^{\mathrm{N}_i}=L_{2yy}^{\mathrm{N}_i}=L_{1xx}^{\mathrm{N}_i}\cong\frac{1}{a_0}\frac{\partial b(c_\mathrm{N})}{\partial c_\mathrm{N}}\bigg|_{c_\mathrm{N}=0}$$

and

$$L_1^{\mathrm{N}_i}\equiv L_{3xx}^{\mathrm{N}_i}=L_{3yy}^{\mathrm{N}_i}=L_{1yy}^{\mathrm{N}_i}=L_{1zz}^{\mathrm{N}_i}=L_{2zz}^{\mathrm{N}_i}=L_{2xx}^{\mathrm{N}_i}\cong\frac{1}{a_0}\frac{\partial a(c_\mathrm{N})}{\partial c_\mathrm{N}}\bigg|_{c_\mathrm{N}=0}$$

are both different values of non-zero (diagonal) elements of the tensor of concentration distortion coefficients $L_{3ij}^{\mathrm{N}_i}$ (i, j = x, y, z) of b.c.c. Fe with interstitial N atoms in only one, the third (with p = 3) sublattice of the octahedral interstices (assuming the Vegard's rule, *i.e.*, practically linear dependences of a and b on c_N at fixed T). Thus, Eq. (12) will also determine the temperature dependence of the ratio b/a.

Thus, the spatial distribution of (nitrogen) atoms in martensitic (b.c.t.-iron–nitrogen) phase obviously affects its tetragonality degree. To analyse this effect adequately, we need to possess detailed information on the parameters of interionic interactions in the (b.c.t.-Fe–N) solid solution.

4. Semi-Empirical Estimation of Interatomic Interaction Energy Parameters for the αFe–N Solid Solution

The objective of the works [98–100] was, in part, the estimation of the microscopic parameters of interionic interactions, both 'direct' '(electro)chemical' (N with N and α-Fe) and indirect, *per se*, strain-induced (N with N), dominating in the αFe–N solid solution. Thus, the calculation of $\tilde{W}^{\mathrm{N}_i\mathrm{N}_i}_{p\,p'}(\mathbf{k})$ was carried out on the assumption that both long-range strain-induced (with energy $V^{\mathrm{N}_i\mathrm{N}_i}_{p\,p'}(\mathbf{R}-\mathbf{R}')$) and short-range '(electro)chemical' (with energy $\varphi^{\mathrm{N}_i\mathrm{N}_i}_{p\,p'}(\mathbf{R}-\mathbf{R}')$) interactions contribute to the energy $W^{\mathrm{N}_i\mathrm{N}_i}_{p\,p'}(\mathbf{R}-\mathbf{R}')$.

To calculate the Fourier components of the strain-induced interaction energies $\tilde{V}^{\mathrm{N}_i\mathrm{N}_i}_{p\,p'}(\mathbf{k})$ using the 'lattice statics method' reported in detail in Refs. [89, 92, 97, 103], a quasi-harmonic model of the b.c.c.-crystal dynamics [97] was used, taking into account dominating (in α-Fe [104]) interactions of metal ions within the first two coordination site shells (central forces in both shells, and non-central ones in the first shell only). The temperature-dependent values of elasticity moduli C_{11}, C_{12}, C_{44} for 'pure' b.c.c. Fe (with the corresponding lattice parameter $a_0 = a_0(T)$ [105]) were taken from Refs. [106, 107]. In addition, $L_3^{\mathrm{N}_i} \cong 0.84$ and $L_1^{\mathrm{N}_i} \cong -0.05$ at $T = 298$ K in accordance with the data of Ref. [108] and in assumption that, in the specimens prepared at this temperature, practically all interstitial N atoms were still lumped in one of the three sublattices of the b.c.t.-Fe octahedral interstices (*e.g.*, inheriting their mutual arrangement in 'homogeneous' austenite).

The following parameters for the b.c.c. Fe with vacancies are also available (at $T = 298$ K): $C_{11} = 273$ GPa, $C_{12} = 150$ GPa, $C_{44} = 106.73$ GPa (*i.e.*, with $\xi < 0$) [109], $a_0 = 2.8663$ Å [110], $L^{v} = -0.016$ [111]. Here, a_0 is a b.c.c.-lattice translation period, C_{11}, C_{12}, C_{44} are the elastic moduli, $\xi \equiv (C_{11} - C_{12} - 2C_{44})/C_{44}$ is an elastic anisotropy factor, L^{v} is a concentration dilatation coefficient of the b.c.c.-Fe lattice due to the presence of vacancies.

To estimate roughly the '(electro)chemical' interactions N–N (*i.e.*, N_i–N_i, N_s–N_s, and N_s–N_i) inside the b.c.c.(t.)-Fe, the following simple model [98–100] is reasonable. The N ions at the octahedral interstices and/or sites of the b.c.t.-Fe interact with each other in almost the same way as N atoms in different molecules containing these atoms (*e.g.*, with the atom–atom N–N-potential for N atoms of the N_2 molecules). The potential of such a (direct) interaction of non-point N ions can be chosen in the form of a model 'point' Lennard-Jones potential with parameters adopted from Ref. [112].

The Fourier components $\tilde{V}^{vv}(\mathbf{k}) = \tilde{W}^{vv}(\mathbf{k}) - \tilde{\varphi}^{vv}_{\mathrm{el.chem}}(\mathbf{k})$ and $\tilde{V}^{v\mathrm{N}_i}_{p'}(\mathbf{k})$ of the strain-induced interaction energies v–v and v–N_i ($V^{vv}(\mathbf{R}-\mathbf{R}')$ and

$V_{p'}^{\upsilon \mathrm{N}_i}(\mathbf{R}-\mathbf{R}')$, respectively) can be calculated based on the theorem that, for the '(electro)chemical' *Me*–*Me* and *υ*–*υ* interactions' potentials, $\varphi^{MeMe}(r) = \varphi^{\upsilon\upsilon}_{\text{el.chem}}(r)$, proved by Harrison [113, 114]. Following Refs. [92, 115], for $T > T_C$, let us use the 'pair potential' for the total *Me*–*Me*-pair interaction in b.c.c.-*Me* crystal (proposed by Machlin [116]):

$$W^{MeMe}(r) \cong \varphi^{MeMe}(r) \approx -\frac{A^{MeMe}}{r^4} + \frac{B^{MeMe}}{r^8}, \qquad (15)$$

where $r = |\mathbf{R} - \mathbf{R}'|$,

$$A^{MeMe} = -\frac{9\varepsilon^0}{4S_4} a_0^4(0\ \mathrm{K}) \cong -0.09939\varepsilon^0 a_0^4(0\ \mathrm{K})\ (S_4 \approx 22.63872),$$

$$B^{MeMe} = -\frac{81\varepsilon^0}{128S_8} a_0^8(0\ \mathrm{K}) \cong -0.0611\varepsilon^0 a_0^8(0\ \mathrm{K})\ (S_8 \approx 10.3552),$$

and ε^0 is the cohesive binding energy; for α-Fe, $\varepsilon^0 \cong -4.28$ eV/atom [117, 118].

Accordingly, for instance,

$$\tilde{w}^{Me\upsilon}(\mathbf{k}) = \tilde{W}^{MeMe}(\mathbf{k}) + \tilde{W}^{\upsilon\upsilon}(\mathbf{k}) - 2\tilde{W}^{Me\upsilon}(\mathbf{k}) \equiv \tilde{w}(\mathbf{k}) \cong$$
$$\cong \tilde{V}^{\upsilon\upsilon}(\mathbf{k}) + \tilde{\varphi}^{\text{mix}}_{\text{el.chem}}(\mathbf{k}) = \tilde{V}^{\upsilon\upsilon}(\mathbf{k}) + \tilde{\varphi}^{MeMe}(\mathbf{k}) + \tilde{\varphi}^{\upsilon\upsilon}_{\text{el.chem}}(\mathbf{k}) - 2\tilde{\varphi}^{Me\upsilon}(\mathbf{k}).$$

The '(electro)chemical' contributions to the *υ*–N$_i$ and *υ*–N$_s$ interactions, which are mainly of the Coulomb type, screened due to the presence of correlations between the distributed charges are acceptable to be neglected henceforth.

Using Eq. (15), one can also estimate the Fourier components $\tilde{W}^{\text{FeFe}}(\mathbf{k})$ and $\tilde{W}^{\text{Fe}\upsilon}(\mathbf{k}) \cong -\tilde{W}^{\text{FeFe}}(\mathbf{k}) \approx -\tilde{W}^{\upsilon\upsilon}(\mathbf{k})$ based on the model assumptions of Girifalco–Weizer [119] and Yamamoto–Doyama [120]. To evaluate the parameters of '(electro)chemical' Fe–N$_s$ and Fe–N$_i$ interactions, we shall assume that these interactions between N and Fe ions at a separation of *r* in martensite are pairwise and centrally symmetric, and the interaction energy can be approximated by the following unified 'interpolation' expression:

$$\varphi^{\text{FeN}}(r) \cong \begin{cases} A^{\text{FeN}} e^{-d_{\text{FeN}} r}, \text{ if } r_{\text{I}}^0 = a_0/2 \le r \le r_{\text{III}}^0 = a_0\sqrt{5}/2; \\ 0, \text{ if } r > r_{\text{III}}^0. \end{cases} \qquad (16)$$

Then, using the conditions of a static mechanical equilibrium for the b.c.c.(t.)-lattice-based interstitial solution [92, 97]:

$$-\sum_{\mathbf{R}} \frac{\partial \varphi^{\text{FeN}_i}(r)}{\partial r} \frac{(R_x - h_{3x})^2}{r} \approx \frac{a_0^3}{4}\left[(C_{11} + C_{12})L_1^{\text{N}_i} + C_{12}L_3^{\text{N}_i}\right], \qquad (17)$$

$$-\sum_{\mathbf{R}} \frac{\partial \varphi^{\mathrm{FeN}_i}(r)}{\partial r} \frac{(R_z - h_{3z})^2}{r} \approx \frac{a_0^3}{4}\left(C_{11}L_3^{\mathrm{N}_i} + 2C_{12}L_1^{\mathrm{N}_i}\right), \tag{18}$$

and taking into account expression (16) and the assumed constraint on the N–Fe-interaction radius, one can find numerically values of the unified (for both N_i and N_s) fitting parameters A^{FeN} and d_{FeN} of function $\varphi^{\mathrm{FeN}}(r)$. Note that the Fe–N interaction 'potential' parameters obtained in this way will be substantially dependent on T due to the temperature dependence of the experimentally determined quantities C_{11}, C_{12}, and a_0.

Using expression (16), one can calculate the Fourier components $\tilde{W}^{\mathrm{FeN}_s}(\mathbf{k})$ and $\tilde{W}_3^{\mathrm{FeN}_i}(\mathbf{k})$ of the interaction energies $W^{\mathrm{FeN}_s}(\mathbf{R} - \mathbf{R}') \cong \cong \varphi^{\mathrm{FeN}_s}(|\mathbf{R} - \mathbf{R}'|)$ and $\tilde{W}^{\mathrm{FeN}_i}(\mathbf{R} - \mathbf{R}') \cong \varphi^{\mathrm{FeN}_i}(|\mathbf{R} - \mathbf{R}' - \mathbf{h}_3|)$ (within the strong assumption that the Fe–N_i and Fe–N_s interaction 'potentials' are identical with $\varphi^{\mathrm{FeN}}(r)$). In addition, based on the obtained values of the Fe–N interaction 'potential' parameters, one can estimate the effective force with which the N atom substituting the b.c.c.(t.)-Fe lattice site would act on the Fe ion occupying some other neighbouring site. This fact opens a way [89, 92, 97] for calculation of the Fourier components $\tilde{V}^{\mathrm{N}_s\mathrm{N}_s}(\mathbf{k})$ and $\tilde{V}_3^{\mathrm{N}_s\mathrm{N}_i}(\mathbf{k})$ of the strain-induced N_s–N_s- and N_s–N_i-interaction energies.

According to Refs. [89, 92], the specific energy associated with the 'expansion' ('compression') of the 'impurity ion' $\alpha = v$, N_s (N_i) introduced into any site (any octahedral interstice) of the b.c.c.-Fe lattice is

$$R^v \cong -\frac{1}{2}\tilde{V}^{vv}(\mathbf{0}) \text{ or } R^{\mathrm{N}_s} \cong -\frac{1}{2}\tilde{V}^{\mathrm{N}_s\mathrm{N}_s}(\mathbf{0}) \quad (R_3^{\mathrm{N}_i} \cong -\frac{1}{2}\tilde{V}_{33}^{\mathrm{N}_i\mathrm{N}_i}(\mathbf{0})),$$

where $\tilde{V}^{vv}(\mathbf{0})$, $\tilde{V}^{\mathrm{N}_s\mathrm{N}_s}(\mathbf{0})$ (and $\tilde{V}_{33}^{\mathrm{N}_i\mathrm{N}_i}(\mathbf{0})$) are the Fourier components (at $\mathbf{k} = \mathbf{0}$) of the respective strain-induced interaction energies.

Thus, one can estimate the energy parameters inherently entering into Eqs. (12) and (13).

5. Discussion of Obtained Results

5.1. Temperature-Dependent Interaction Energy

As shown in Refs. [98–100], the Fourier components $\tilde{W}_{33}^{\mathrm{N}_i\mathrm{N}_i}(\mathbf{k})$ and especially $\tilde{V}_{33}^{\mathrm{N}_i\mathrm{N}_i}(\mathbf{k})$ depend significantly on temperature T. As an example, Fig. 6 shows the temperature dependences of the values $\tilde{W}^{\mathrm{FeN}_s}(\mathbf{0})$ and $\tilde{W}_3^{\mathrm{FeN}_i}(\mathbf{0})$. These Fourier components have the meaning of the total interaction energy of one selected N atom substituting a site or intruding into an octahedral interstice of the b.c.t.-Fe, respectively, with all other Fe ions at the sites. As seen from Fig. 6, these energy parameters $\tilde{W}^{\mathrm{FeN}_s}(\mathbf{0})$ and $\tilde{W}_3^{\mathrm{FeN}_i}(\mathbf{0})$ can increase overall (but non-monotonically) with increasing temperature.

5.2. Correlation of the Spatial Redistribution of Interstitial Atoms in the Solid Solution with Its Tetragonality

Solving Eq. (12), we have to take into account the temperature dependences of energy parameters (entering to it), since both the elasticity moduli $C_{IJ}(T)$ and lattice parameter $a_0(T)$ of the 'impurity-free' b.c.c.-Fe are dependent on T.

Ignoring magnetic effects, Fig. 7 (left and right) demonstrates the $c_{N_i}\big|_{c_N} = c_{N_i}(T)$ curves for two different values of the total N-atomic content c_N. As follows from Fig. 7, even for $T \to 0$ K ($\ll T_C$), part of the N atoms substitutes the b.c.t.-Fe lattice sites in equilibrium: $c_{N_i}\big|_{c_N=10\%}^{T\to 0\text{ K}} \cong 9\%$ and $c_{N_i}\big|_{c_N=12\%}^{T\to 0\text{ K}} \cong 9.9\%$. It means that, for N content of $10\% \le c_N \le 12\%$ (*i.e.*, close to that in α″-$Fe_{16}N_2$), ≅82.5–90% (≅10–17.5%) of nitrogen atoms may be resided in the octahedral interstices (sites) for $T \to 0$ K.

On further increase of T, c_{N_i} decreases that results to the fact (clear seen from Fig. 7) that the 'high-temperature' value of c_{N_i} can be by more than 10% less than its 'low-temperature' value. Particularly, $c_{N_i}\big|_{c_N=10\%}^{T\approx 1000\text{ K}} \cong 8\%$ and $c_{N_i}\big|_{c_N=12\%}^{T\approx 1000\text{ K}} \cong 9\%$, that is ≅75–80% (≅20–25%) of N atoms can occupy interstitial (substitutional) positions.

Consequently (see Eq. (14)), with increasing temperature, a noticeable decrease in the degree of tetragonality of the b.c.t.-Fe–N solution can take place (due to the redistribution of N atoms amongst one of the octahedral interstices' sublattices of b.c.t.-Fe and its vacancy-filled site lattice).

In the temperature range $T \in (4.2\text{ K}; 300\text{ K})$, the non-monotonicity of the $c_{N_i} = c_{N_i}(T)$ function is possible. Apparently, the shape of function $c_{N_i}(T)$ here is explained here, in essence, by the non-monotonic temperature dependence of the energy parameters in Eq. (12). However, due to the smallness of these non-monotonicity effects, it is unlikely that such a behaviour of $c_{N_i}(T)$ can cause a noticeable (in the experiment) change in tetragonality of iron–nitrogen martensite (for $4.2\text{ K} < T < 300\text{ K}$).

Some quantitative disagreements between the available experimental

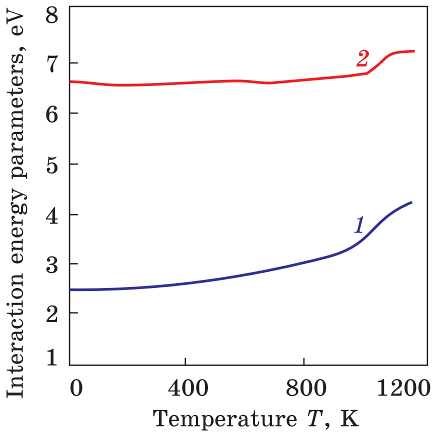

Fig. 6. The temperature-dependent absolute values of the Fourier components $\tilde{W}^{\text{FeN}_s}(0)$ (curve *1*) and $\tilde{W}_3^{\text{FeN}_i}(0)$ (curve *2*) of the interaction energies $W^{\text{FeN}_s}(\mathbf{R}-\mathbf{R}') \cong \varphi^{\text{FeN}_s}(|\mathbf{R}-\mathbf{R}'|)$ and $\tilde{W}_3^{\text{FeN}_i}(\mathbf{R}-\mathbf{R}') \cong \varphi^{\text{FeN}_i}(|\mathbf{R}-\mathbf{R}'-\mathbf{h}_3|)$, respectively

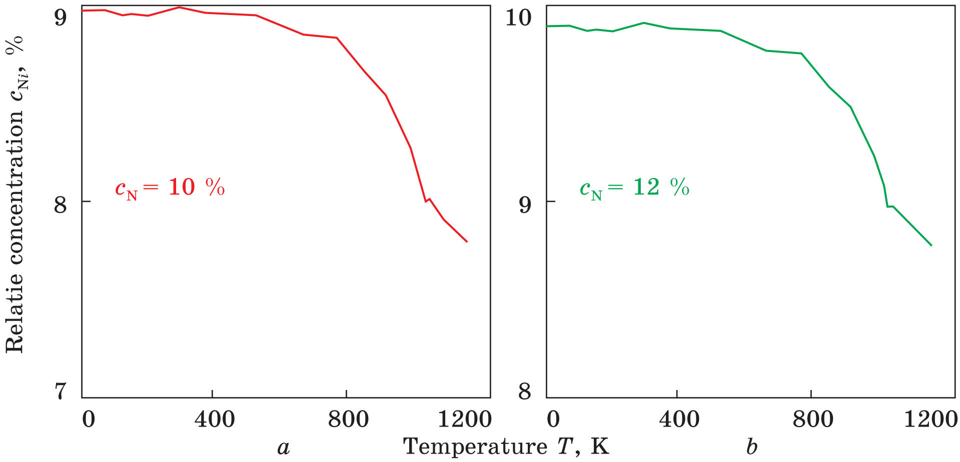

Fig. 7. The temperature dependences of 'relative' concentration c_{N_i} of nitrogen atoms remaining as interstitials in only one sublattice of octahedral interstices in the host b.c.t.-Fe crystal lattice for two values of the total content of N atoms: $c_N = 10\%$ (left) and 12% (right)

and obtained theoretical results concerning the degree of tetragonality could be due, in part, to the use in the present study of restriction on the possibility of formation of complexions of N atoms at the b.c.t.-Fe–N solid solution sites, the concentration of which (in contrast to other point defects) should decrease overall with decreasing temperature. It is the case that the transition of additional N atoms from interstices to the site-'traps' is capable of leading to their local disordering, and as a result, to much more pronounced decrease (possibly, non-monotonic) of the overall degree of tetragonality of the solution lattice.

5.3. Ratio of Residual and Thermally Activated Vacancies

It can be seen from Fig. 8 (see also Eq. (13)) that the concentration of site vacancies in the α′Fe–N alloy lattice, where the N atoms in the octahedral interstices (and partially at the sites) of b.c.t.-Fe are maximally ordered in the α″-$Fe_{16}N_2$-type phase, can substantially increase (even for T = const) with increasing the total concentration of N atoms intruded into α-Fe, so that it will no longer be possible to neglect completely the combination of vacant sites into the divacancies as another entropy–geometric factor of alloy thermodynamics). This agrees with theoretical predictions in Refs. [101, 121] for point defects in monoatomic crystals and diluted binary alloys, with results of preliminary study of the dependence of the concentration site monovacancies υ on the increase (in a certain range) of the concentration of interstitial nonmetal X (X = N, H) atoms into octahedral interstices of f.c.c.-Fe (with-

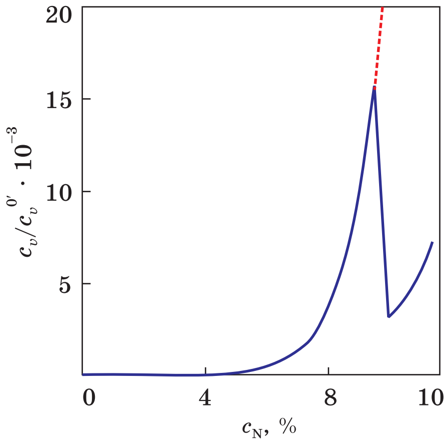

Fig. 8. The ratio $c_v/c_v^{0'}$ (solid curve) *vs*. the total concentration c_N of interstitial nitrogen atoms (for T = 1173 K); dashed line shows the hypothetical case of $c_{N_s} \equiv 0$.

out account their transition to the sites, *i.e.*, for $c_{X_s} \equiv 0$) [122], and others (see Ref. [91] and references therein).

The 'enormous' inflection of the solid curve ($c_v/c_v^{0'}$) in Fig. 8 corresponds approximately to those values of the 'relative' concentration c_N, at which (for T = 1173 K) a spontaneous transition of part of the N atoms from octahedral interstices to b.c.t.-Fe sites takes place. Apparently, during this process, the N atoms occupy part of the vacant b.c.t.-lattice sites, and thereby, sharply decrease the number of (residual) vacancies v in the solution (see Fig. 8). For comparison, dashed line in Fig. 8 depicts a hypothetical dependence $c_v/c_v^{0'}$ on c_N, which is obtained without taking into account the transition of N atoms from interstices to sites (*i.e.*, for $c_{N_s} \equiv 0$). As seen from comparison of the solid and dashed lines in Fig. 8, the transition of a significant fraction of N atoms to the b.c.t.-Fe lattice sites at the fixed temperature is possible only starting from a certain concentration c_N of interstitial atoms (and somewhat higher).

6. Summary, Conclusions, Challenges

Reviewing and analysing the experimental and theoretical literature data dealing with metallic phases for permanent magnets, a special attention is paid to studying the martensitic α″-Fe$_{16}$N$_2$-type phase due to its giant saturation magnetization, which exhibits it as a prospective material for fabrication of rare-earth-free permanent magnets without containing the critical chemical elements (practically non-renewable on the Earth). Among available in the literature attempts to explain the 'magnetic mystery' of α″-Fe$_{16}$N$_2$ phase, we stress on the structural contribution, *i.e.*, the specific arrangement of nitrogen atoms within the host iron crystal lattice, to the magnetic characteristics.

In order to develop the statistical-thermodynamic model of 'hybrid' b.c.t.-lattice-based interstitial–substitutional solid solution containing non-metal impurity atoms at both the interstices and the sites of the metal lattice, we took into account the discrete (atomic-crystalline) lattice structure, the anisotropy of its elasticity, the 'blocking' and strain-induced ('size') effects in the interactions of all atoms, which constitute the system. Adapting the model for a maximally ordered α''-$Fe_{16}N_2$-type structure with N atoms at the interstitial and substitutional positions in b.c.t.-Fe, we obtained the single-site occupation-probability functions for N-atomic distribution assuming some reasonable approximations. A set of equations is derived for calculation of the thermodynamically-equilibrium concentrations of impurity N atoms in the interstices as compared to those moved to sites as well as of vacancies at the sites. To solve these equations, we have to possess information (mainly extract from the available literature data) on the temperature- and concentration-dependent interatomic-interaction energies' parameters. Their adequate magnitudes are necessary condition for obtaining reasonable and physically argued results.

The calculated results on the temperature-dependent content of impurity nitrogen atoms in the octahedral interstices of the b.c.t.-Fe lattice confirm the expected predictions: even at a zero temperature, not all nitrogen atoms remain in the interstices, part of them move to the vacant sites of the host lattice. Further increasing the temperature just intensifies (makes stronger) this trend (process): for the nitrogen concentration within the range $10–12\%$, *i.e.*, close to the $Fe_{16}N_2$ composition, the part impurity (N) atoms found in the sites of the host (Fe) lattice rises from $\cong$10–17.5% (for $T \approx 0$ K) to $\cong$20–25% (for $T \approx 1000$ K), and even higher at higher temperatures. Since the spatial arrangement of N atoms in the b.c.t.-Fe–N martensite correlates with its tetragonality, we can conclude that, by tuning (controlling) the temperature, one can manipulate the degree of tetragonality (for $T > T_C = T_C(c_{N_i}, c_{N_s} + c_v)$ and, tentatively, even for $T < T_C$).

The non-monotonic dependence of the site-vacancies' concentration on the total content of impurity N atoms in Fe–N is observed. Initially, with increasing the nitrogen content, the vacancy concentration substantially increases (even for T = const). However, then (when part of nitrogen atoms spontaneously jump from the octahedral interstices into the host-lattice sites), the number of (residual) vacancies sharply decreases as a result of the occupation of virtually vacant sites by the N atoms. Such an 'abrupt' transition (of a significant part of N atoms to the b.c.t.-Fe lattice sites) at the fixed temperature is possible only at a certain concentration of interstitial impurity N atoms and somewhat higher ones, however, lower the stoichiometric composition in $Fe_{16}N_2$.

Based on the present work, its methodology, and obtained results, one of the next stages (challenges) in the studying the α''-$Fe_{16}N_2$-phase for much more clear understanding and explaining its properties and, particularly, 'magnetic mystery' is the explicit including of the spin exchange-interaction of Fe atoms in the mixing (interchange) energy expression to obtain results dependent on both atomic and magnetic orderings at the given external impacts (temperature, pressure, or appropriate deformation).

Acknowledgement. Authors are grateful to the National Research Foundation of Ukraine (NRFU) for the Grant support of the Project 'Controlling the Atomic Distribution for the Functionalization of the Hybrid $Fe_{16}N_2$-Martensite Phase Based Materials as an Alternative to Permanent Magnets Made of Rare Earth Intermetallics or Permendur' (State Reg. No. 0120U104061) within the NRFU Competition 'Leading and Young Scientists Research Support' (application ID 2020.02/0191; contract No. 53/02.2020 as from 27.10.2020).

REFERENCES

1. J.-P. Wang, Environment-Friendly Bulk $Fe_{16}N_2$ Permanent Magnet: Review and Prospective, *J. Magn. Magn. Mater.*, **497**: 165962 (2020); https://doi.org/10.1016/j.jmmm.2019.165962
2. J. Cui, M. Kramer, L. Zhou, F. Liu, A. Gabay, G. Hadjipanayis, B. Balasubramanian, and D. Sellmyer, Current Progress and Future Challenges in Rare-Earth-Free Permanent Magnets, *Acta Mat.*, **158**: 118 (2018); https://doi.org/10.1016/j.actamat.2018.07.049
3. J.T. Dreyer, China's Monopoly on Rare Earth Elements — and Why We Should Care (Philadelphia: Foreign Policy Research Institute: October 7, 2020); https://www.fpri.org/article/2020/10/chinas-monopoly-on-rare-earth-elements-and-why-we-should-care
4. N.A. Mancheri, Chinese Monopoly in Rare Earth Elements: Supply–Demand and Industrial Applications, *China Report*, **48**, No. 4: 449 (2013); https://doi.org/10.1177/0009445512466621
5. L.H. Lewis and F. Jiménez-Villacorta, Perspectives on Permanent Magnetic Materials for Energy Conversion and Power Generation, *Metall. Mater. Trans. A*, **44**: 2 (2013); https://doi.org/10.1007/s11661-012-1278-2
6. M.J. Kramer, R.W. McCallum, I.A. Anderson, and S. Constantinides, Prospects for Non-Rare Earth Permanent Magnets for Traction Motors and Generators, *JOM*, **64**: 752 (2012); https://doi.org/10.1007/s11837-012-0351-z
7. O. Gutfleisch, M.A. Willard, E. Brück, C.H. Chen, S.G. Sankar, and J.P. Liu, Magnetic Materials and Devices for the 21st Century: Stronger, Lighter, and More Energy Efficient, *Adv. Mater.*, **23**, No. 7: 821 (2011); https://doi.org/10.1002/adma.201002180
8. T.M. Radchenko, V.A. Tatarenko, and S.M. Bokoch, Diffusivities and Kinetics of Short-Range and Long-Range Orderings in Ni–Fe Permalloys, *Metallofiz. Noveishie Tekhnol.*, **28**, No. 12: 1699 (2006).
9. T.M. Radchenko and V.A. Tatarenko, Atomic-Ordering Kinetics and Diffusivities in Ni–Fe Permalloy, *Defect Diffus. Forum*, **273–276**: 525 (2008); https://doi.org/10.4028/www.scientific.net/DDF.273-276.525
10. V.A. Tatarenko and T.M. Radchenko, The Application of Radiation Diffuse Scattering to the Calculation of Phase Diagrams of F.C.C. Substitutional Alloys, *Intermetallics*, **11**, Nos. 11–12: 1319 (2003); https://doi.org/10.1016/S0966-9795(03)00174-2

11. S.M. Bokoch and V.A. Tatarenko, A Semi-Empirical Parameterization of Interatomic Interactions Based on the Statistical-Thermodynamic Analysis of the Data on Radiation Diffraction and Phase Equilibria in F.C.C.-Ni–Fe Alloys, *Solid State Phenom.*, **138**: 303 (2008);
https://doi.org/10.4028/www.scientific.net/SSP.138.303
12. V.A. Tatarenko, S.M. Bokoch, V.M. Nadutov, T.M. Radchenko, and Y.B. Park, Semi-Empirical Parameterization of Interatomic Interactions and Kinetics of the Atomic Ordering in Ni–Fe–C Permalloys and Elinvars, *Defect Diffus. Forum*, **280**: 29 (2008);
https://doi.org/10.4028/www.scientific.net/DDF.280-281.29
13. T.M. Radchenko and V.A. Tatarenko, Fe–Ni Alloys at High Pressures and Temperatures: Statistical Thermodynamics and Kinetics of the $L1_2$ or $D0_{19}$ Atomic Order, *Usp. Fiz. Met.*, **9**, No. 1: 1 (2008) (in Ukrainian);
https://doi.org/10.15407/ufm.09.01.001
14. V.A. Tatarenko, T.M. Radchenko, and V.M. Nadutov, Parameters of Interatomic Interaction in a Substitutional Alloy F.C.C. Ni–Fe According to Experimental Data about the Magnetic Characteristics and Equilibrium Values of Intensity of a Diffuse Scattering of Radiations, *Metallofiz. Noveishie Tekhnol.*, **25**, No. 10: 1303 (2003) (in Ukrainian).
15. R.C. O'Handley, *Modern Magnetic Materials: Principles and Applications* (New York: Wiley: 2000).
16. K.H. Jack, The Iron–Nitrogen System: the Preparation and the Crystal Structures of Nitrogen–Austenite (γ) and Nitrogen–Martensite (α'), *Proc. R. Soc. London, Ser. A*, **208**: 200 (1951);
https://doi.org/10.1098/rspa.1951.0154
17. K.H. Jack, The Occurrence and the Crystal Structure of α''-Iron Nitride; a New Type of Interstitial Alloy Formed during the Tempering of Nitrogen–Martensite, *Proc. Roy. Soc. London, Ser. A*, **208**: 216 (1951);
https://doi.org/10.1098/rspa.1951.0155
18. T.K. Kim and M. Takahashi, New Magnetic Material Having Ultrahigh Magnetic Moment, *Appl. Phys. Lett.*, **20**, No. 12: 492 (1972);
https://doi.org/10.1063/1.1654030
19. X. Hang, M. Matsuda, J.T. Held, K.A. Mkhoyan, and J.-P. Wang, Magnetic Structure of $Fe_{16}N_2$ Determined by Polarized Neutron Diffraction on Thin-Film Samples, *Phys. Rev. B*, **102**, No. 10: 104402 (2020);
https://doi.org/10.1103/PhysRevB.102.104402
20. L. Feng, D. Zhang, F. Wang, L. Dong, S. Chen, J. Liu, and X. Hui, A New Structure of the Environment-Friendly Material $Fe_{16}N_2$, *Chem. Eng. Trans.*, **61**: 1501 (2017);
https://doi.org/10.3303/CET1761248
21. Y. Sugita, H. Takahashi, M. Komuro, K. Mitsuoka, and A. Sakuma, Magnetic and Mössbauer Studies of Single-Crystal $Fe_{16}N_2$ and Fe–N Martensite Films Epitaxially Grown by Molecular Beam Epitaxy, *J. Appl. Phys.*, **76**, No. 10: 6637 (1994);
https://doi.org/10.1063/1.358157
22. N. Ji, V. Lauter, X. Zhang, H. Ambaye, and J.-P. Wang, Strain Induced Giant Magnetism in Epitaxial $Fe_{16}N_2$ Thin Film, *Appl. Phys. Lett.*, **102**, No. 7: 072411 (2013);
https://doi.org/10.1063/1.4792706
23. J. Liu, G. Guo, X. Zhang, F. Zhang, B. Ma, and J.-P. Wang, Synthesis of α''-$Fe_{16}N_2$ Foils with an Ultralow Temperature Coefficient of Coercivity for Rare-Earth-Free Magnets, *Acta Mat.*, **184**: 143 (2020);

https://doi.org/10.1016/j.actamat.2019.11.052
24. N. Ji, X. Liu, and J.-P. Wang, Theory of Giant Saturation Magnetization in α″-$Fe_{16}N_2$: Role of Partial Localization in Ferromagnetism of 3*d* Transition Metals, *New J. Phys.*, **12**: 063032 (2010);
https://doi.org/10.1088/1367-2630/12/6/063032
25. J.-P. Wang, N. Ji, X. Liu, Y. Xu, C. Sanchez-Hanke, Y. Wu, F.M.F. de Groot, L.F. Allard, and E. Lara-Curzio, Fabrication of $Fe_{16}N_2$ Films by Sputtering Process and Experimental Investigation of Origin of Giant Saturation Magnetization in $Fe_{16}N_2$, *IEEE Trans. Magn.*, **48**, No. 5: 1710 (2012);
https://doi.org/10.1109/TMAG.2011.2170156
26. S. Bhattacharjee and S.-C. Lee, First-Principles Study of the Complex Magnetism in $Fe_{16}N_2$, *Sci. Rep.*, **9**: 8381 (2019);
https://doi.org/10.1038/s41598-019-44799-8
27. K.H. Jack, The Synthesis, Structure, and Characterization of α″-$Fe_{16}N_2$, *J. Appl. Phys.*, **76**: 6620 (1994);
https://doi.org/10.1063/1.358482
28. K.H. Jack, The Synthesis and Characterization of Bulk α″-$Fe_{16}N_2$, *J. Alloys Compd.*, **222**, Nos. 1, 2: 160 (1995);
https://doi.org/10.1016/0925-8388(94)04901-7
29. H.A. Wriedt, N.A. Gokcen, and R.H. Nafziger, The Fe–N (Iron–Nitrogen) System, *Bull. Alloy Phase Diagrams*, **8**: 355 (1987);
https://doi.org/10.1007/BF02869273
30. E.H.D.M. van Voorthuysen, D.O. Boerma, and N.C. Chechenin, Low-Temperature Extension of the Lehrer Diagram and the Iron–Nitrogen Phase Diagram, *Metall. Mater. Trans. A*, **33**: 2593 (2002);
https://doi.org/10.1007/s11661-002-0380-2
31. M. Naito, K. Uehara, R. Takeda, Y. Taniyasu, and H. Yamamoto, Growth of Iron Nitride Thin Films by Molecular Beam Epitaxy, *J. Crystal Growth*, **415**: 36 (2015);
https://doi.org/10.1016/j.jcrysgro.2014.12.022
32. S. Grachev, D.M. Borsa, S. Vongtragool, and D.O Boerma, The Growth of Epitaxial Iron Nitrides by Gas Flow Assisted MBE, *Surf. Sci.*, **482–485**, Pt. 2: 802 (2001);
https://doi.org/10.1016/S0039-6028(00)01084-0
33. T. Weber, L. de Wit, F.W. Saris, and P. Schaaf, Search for Giant Magnetic Moments in Ion-Beam-Synthesized α″-$Fe_{16}N_2$, *Thin Solid Films*, **279**, Nos. 1–2: 216 (1996);
https://doi.org/10.1016/0040-6090(95)08176-3
34. E. Leroy, C.D. Mariadassou, H. Bernas, O. Kaitasov, and R. Krishnan, The Road to $Fe_{16}N_2$ Formation in N^+ Implanted ^{57}Fe Enriched Films, *Appl. Phys. Let.*, **67**, No. 4: 560 (1995);
https://doi.org/10.1063/1.115169
35. K. Nakajima and S. Okamoto, Nitrogen-Implantation-Induced Transformation of Iron to Crystalline $Fe_{16}N_2$ in Epitaxial Iron Films, *Appl. Phys. Lett.*, **54**, No. 25: 2536 (1989);
https://doi.org/10.1063/1.101543
36. S. Okamoto, O. Kitakami, and Y. Shimada, α″-$Fe_{16}N_2$ Phase Epitaxially Grown by Sputter Beam Method, *J. Appl. Phys.*, **79**, No. 4: 5250 (1996);
https://doi.org/10.1063/1.361301
37. Z.-Y. Yao, H. Jiang, Z.-K. Liu, D.-D. Huang, F.-G. Qin, S.-C. Zhu, and Y.-X. Sun, *J. Magn. Magn. Mater.*, **177–181**, Pt. 2: 1291 (1998);
https://doi.org/10.1016/S0304-8853(97)01020-2

38. D.C. Sun, E.Y. Jiang, M.B. Tian, C. Lin, and X.X. Zhang, Epitaxial Single crystal $Fe_{16}N_2$ Films Grown by Facing Targets Sputtering, *J. Appl. Phys.*, **79**, No. 4: 5440 (1996);
https://doi.org/10.1063/1.361843
39. N. Ji, M.S. Osofsky, V. Lauter, L.F. Allard, X. Li, K.L. Jensen, H. Ambaye, E. Lara-Curzio, and J.-P. Wang, Perpendicular Magnetic Anisotropy and High Spin-Polarization Ratio in Epitaxial Fe–N Thin Films, *Phys. Rev. B*, **84**, No. 24: 245310 (2011);
https://doi.org/10.1103/PhysRevB.84.245310
40. X. Zhang, K. Nomura, and J.-P. Wang, New Insight on the Mössbauer Spectra for $Fe_{16}N_2$ Thin Films with High Saturation Magnetization, *Jap. J. Appl. Phys.*, **58**, No. 12: 120907 (2019);
https://doi.org/10.7567/1347-4065/ab5273
41. M.A. Brewer, C.J. Echer, K.M. Krishnan, T. Kobayashi, and A. Nakanishi, Magnetic and Physical Microstructure of $Fe_{16}N_2$ Films Grown Epitaxially on Si(001), *J. Appl. Phys.*, **81**, No. 8: 4128 (1997);
https://doi.org/10.1063/1.365102
42. H. Takahashi, H. Shoji, and M. Takahashi, Structure and Magnetic Moment of $Fe_{16}N_2$ Sputtered Film, *J. Magn. Magn. Mater.*, **174**, Nos. 1–2: 57 (1997);
https://doi.org/10.1016/S0304-8853(97)00213-8
43. M. Takahashi, H. Shoji, H. Takahashi, H. Nashi, and T. Wakiyama, Magnetic Moment of α''-$Fe_{16}N_2$ Films, J. Appl. Phys., **76**, No. 10: 6642 (1994);
https://doi.org/10.1063/1.358431
44. Y.F. Jiang, J.M. Liu, P.K. Suri, G. Kennedy, N.N. Thadhani, D.J. Flannigan, and J.P. Wang, Preparation of an α''-$Fe_{16}N_2$ Magnet via a Ball Milling and Shock Compaction Approach, *Adv. Eng. Mat.*, **18**, No. 6: 1009 (2015);
https://doi.org/10.1002/adem.201500455
45. Y. Jiang, V. Dabade, L.F. Allard, E.L.-C., R. James, and J.-P. Wang, Synthesis of α''-$Fe_{16}N_2$ Compound Anisotropic Magnet by the Strained-Wire Method, *Phys. Rev. Applied*, **6**, No. 2: 024013 (2016);
https://doi.org/10.1103/PhysRevApplied.6.024013
46. H. Shinno and K. Saito, Effects of Film Thickness on Formation Processes of $Fe_{16}N_2$ in Nitrogen Ion-Implanted Fe Films, *Surf. Coat. Technol.*, **103–104**: 129 (1998);
https://doi.org/10.1016/S0257-8972(98)00388-0
47. J.M.D. Coey, K. O'Donnell, Q. Qinian, E. Touchais, and K.H. Jack, The Magnetization of Alpha″$Fe_{16}N_2$, *J. Phys.: Condens. Matter*, **6**, No. 4: L23 (1994);
https://doi.org/10.1088/0953-8984/6/4/001
48. J.M.D. Coey, The Magnetization of Bulk $\alpha'Fe_{16}N_2$, *J. Appl. Phys.*, **76**, No. 10: 6632 (1994);
https://doi.org/10.1063/1.358156
49. M.Q. Huang, W.E. Wallace, S. Simizu, and S.G.Sankar, Magnetism of α'-FeN Alloys and α''-($Fe_{16}N_2$) Fe Nitrides, *J. Magn. Magn. Mater.*, **135**, No. 2: 226 (1994);
https://doi.org/10.1016/0304-8853(94)90350-6
50. X. Bao and R.M. Metzger, Synthesis and Properties of α''-$Fe_{16}N_2$ in Magnetic Particles, *J. Appl. Phys.*, **75**, No. 10: 5870 (1994);
https://doi.org/10.1063/1.356988
51. H. Takahashi, M. Komuro, M. Hiratani, and M. Igarashi, Anomalous Hall Resistivities of Single-Crystal $Fe_{16}N_2$ and Fe–N Martensite Films Epitaxially Grown by Molecular Beam Epitaxy, *J. Appl. Phys.*, **84**, No. 3: 1493 (1998);
https://doi.org/10.1063/1.368253

52. H. Tanaka, S. Nagakura, Y. Nakamura, and Y. Hirotsu, Electron Crystallography Study of Tempered Iron–Nitrogen Martensite and Structure Refinement of Precipitated α″-$Fe_{16}N_2$, *Acta Mat.*, **45**, No. 4: 1401 (1997); https://doi.org/10.1016/S1359-6454(96)00270-4
53. Y. Sugita, H. Takahashi, M. Komuro, and M. Igarashi, Magnetic and Electrical Properties of Single-Phase, Single-Crystal $Fe_{16}N_2$ Films Epitaxially Grown by Molecular Beam Epitaxy, *J. Appl. Phys.*, **79**, No. 8: 5576 (1996); https://doi.org/10.1063/1.362246
54. E. Kita, K. Shibata, Y. Sasaki, M. Kishimoto, and H. Yanagihara, Magnetic Anisotropy in Spherical $Fe_{16}N_2$ Core–Shell Nanoparticles Determined by Torque Measurements, *AIP Advances*, **7**, No. 5: 056212 (2017); https://doi.org/10.1063/1.4974276
55. S. Kikkawa, A. Yamada, Y. Masubuchi, and T. Takeda, Fine $Fe_{16}N_2$ Powder Prepared by Low-Temperature Nitridation, *Mater. Res. Bull.*, **43**, No. 12: 3352 (2008); https://doi.org/10.1016/j.materresbull.2008.02.008
56. T. Ogawa, Y. Ogata, R. Gallage, N. Kobayashi, N. Hayashi, Y. Kusano, S. Yamamoto, K. Kohara, M. Doi, and M. Takano, Challenge to the Synthesis of α″-$Fe_{16}N_2$ Compound Nanoparticle with High Saturation Magnetization for Rare Earth Free New Permanent Magnetic Material, *Appl. Phys. Express*, **6**, No. 7: 073007 (2013); https://doi.org/10.7567/APEX.6.073007
57. T. Kojima, S. Kameoka, M. Mizuguchi, K. Takanashi, and A.-P. Tsai, FeNi and $Fe_{16}N_2$ Magnets Prepared Using Leaching, *Mater. Trans.*, **60**, No. 6: 1066 (2019); https://doi.org/10.2320/matertrans.M2019019
58. J. Liu, G. Guo, F. Zhang, Y. Wu, B. Ma, and J.-P. Wang, Synthesis of α″-$Fe_{16}N_2$ Ribbons with a Porous Structure, *Nanoscale Adv.*, **1**, No. 4: 1337 (2019); https://doi.org/10.1039/C9NA00008A
59. Y. Sugita, K. Mitsuoka, M. Komuro, H. Hoshiya, Y. Kozono, and M. Hanazono, Giant Magnetic Moment and Other Magnetic Properties of Epitaxially Grown $Fe_{16}N_2$ Single-Crystal Films, *J. Appl. Phys.*, **70**, No. 10: 5977 (1991); https://doi.org/10.1063/1.350067
60. H. Jiang, K. Tao, and H. Li, *J. Phys.: Condens. Matter.*, **6**, No. 18: L279 (1994); https://doi.org/10.1088/0953-8984/6/18/004
61. I. Fall and J.-M.R. Genin, Mössbauer Spectroscopy Study of the Aging and Tempering of High Nitrogen Quenched Fe–N Alloys: Kinetics of Formation of $Fe_{16}N_2$ Nitride by Interstitial Ordering in Martensite, *Metall. Mater. Trans. A*, **27**: 2160 (1996); https://doi.org/10.1007/BF02651871
62. X. Zhang, M. Yang, Y. Jiang, L.F. Allard, and J.-P. Wang, Thermal Stability of Partially Ordered $Fe_{16}N_2$ Film on Non-Magnetic Ag under Layer, *J. Appl. Phys.*, **115**, No. 17, 17A767 (2014); https://doi.org/10.1063/1.4869065
63. Y. Shinpei, R. Gallage, Y. Ogata, Y. Kusano, N. Kobayashi, T. Ogawa, N. Hayashi, K. Kohara, M. Takahashi, and M. Takano, Quantitative Understanding of Thermal Stability of α″-$Fe_{16}N_2$, *Chem. Commun.*, **49**, No. 70: 7708 (2013); https://doi.org/10.1039/C3CC43590C
64. M.H. Han, W.J. Kim, E.K. Lee, H. Kim, S. Lebègue, and J.J Kozak, Theoretical Study of the Microscopic Origin of Magnetocrystalline Anisotropy in $Fe_{16}N_2$ and Its Alloys: Comparison with the Other $L1_0$ Alloys, *J. Phys.: Condens. Matter.*, **32**, No. 3: 035801 (2020); https://doi.org/10.1088/1361-648X/ab422c

65. N.J. Szymanski, V. Adhikari, M.A. Willard, P. Sarin, D. Gall, and S.V. Khare, Prediction of Improved Magnetization and Stability in $Fe_{16}N_2$ through Alloying, *J. Appl. Phys.*, **126**, No. 9: 093903 (2019);
https://doi.org/10.1063/1.5109571
66. M. Kopcewicz, J. Jagielski, G. Gawlik, and A. Grabias, Role of Alloying Elements in the Stability of Nitrides in Nitrogen-Implanted α-Fe, *J. Appl. Phys.*, **78**, No. 2: 1312 (1995);
https://doi.org/10.1063/1.360373
67. R. Gupta R, A. Tayal, S.M. Amir, M. Gupta, A. Gupta, M. Horisberger, and J. Stahn, Formation of Iron Nitride Thin Films with Al and Ti Additives, *J. Appl. Phys.* **111**, No. 10: 103520 (2012);
https://doi.org/10.1063/1.4718579
68. H.Y. Wang and E.Y. Jiang, Enhancement of the thermal stability of $Fe_{16}N_2$ by Ti Addition, *J. Phys.: Condens. Matter*, **9**, No. 13: 2739 (1997);
https://doi.org/10.1088/0953-8984/9/13/011
69. L. Ke, K.D. Belashchenko, M. van Schilfgaarde, T. Kotani, and V.P. Antropov, Effects of Alloying and Strain on the Magnetic Properties of $Fe_{16}N_2$, *Phys. Rev. B*, **88**, No. 2: 024404 (2013);
https://doi.org/10.1103/PhysRevB.88.024404
70. Y. Jiang, B. Himmetoglu, M. Cococcioni, and J.-P. Wang, DFT Calculation and Experimental Investigation of Mn Doping Effect in $Fe_{16}N_2$, *AIP Adv.*, **6**, No. 5: 056007 (2016);
https://doi.org/10.1063/1.4943059
71. M. Takahashi, H. Takahashi, H. Nashi, H. Shoji, and T. Wakiyama, M. Kuwabara, Structure and Magnetic Moment of α''-$Fe_{16}N_2$ Compound Films: Effect of Co and H on Phase Formation, *J. Appl. Phys.*, **79**, No. 8: 5564 (1996);
https://doi.org/10.1063/1.362244
72. Y. Sun, Y.-X. Yao, M.C. Nguyen, C.Z. Wang, K.M. Ho, and V. Antropov, Spatial Decomposition of Magnetic Anisotropy in Magnets: Application to Doped $Fe_{16}N_2$, *Phys. Rev. B*, **102**, No. 3: 134429 (2020);
https://doi.org/10.1103/PhysRevB.102.134429
73. I. Khan, S. Park, and J. Hong, Magnetic Properties of $Fe_{16-x}(Ta/W)_xN_2$ Ternary Alloy: First Principles and Atomistic Simulations, *J. Phys.: Condens. Matter*, **32**, No. 2: 025801 (2019);
https://doi.org/10.1088/1361-648X/ab3ffa
74. N. Ishiwata, C. Wakabayashi, and H. Urai, Soft Magnetism of High-Nitrogen-Concentration FeTaN Film, *J. Appl. Phys.*, **69**, No. 8: 5616 (1991);
https://doi.org/10.1063/1.347940
75. K. Nakanishi, O. Shimizu, and S. Yoshida, Magnetic Properties of Fe–X–N (X = = Zr, Hf, Nb, Ta) Films, *IEEE Translation J. Magn. Jap.*, **7**, No. 2: 128 (1992);
https://doi.org/10.1109/TJMJ.1992.4565344
76. K. Nago, H. Sakakima, and K. Ihara, Microstructures and Magnetic Properties of Fe–(Ta,Nb,Zr)–N Alloy Films, *IEEE Translation J. Magn. Jap.*, **7**, No. 2: 119 (1992);
https://doi.org/10.1109/TJMJ.1992.4565343
77. M. Widenmeyer, L. Shlyk, A. Senyshyn, R. Mönig, and R. Niewa, Structural and Magnetic Characterization of Single-Phase Sponge-Like Bulk α''-$Fe_{16}N_2$, *Z. Anorg. Allg. Chem.*, **641**, No. 2: 348 (2015);
https://doi.org/10.1002/zaac.201500013
78. J.M.D. Coey and P.A.I. Smith, Magnetic Nitrides, *J. Magn. Magn. Mater.*, **200**: 404 (1999);
https://doi.org/10.1016/S0304-8853(99)00429-1

79. S. Bhattacharyya, Iron Nitride Family at Reduced Dimensions: A Review of Their Synthesis Protocols and Structural and Magnetic Properties, *J. Phys. Chem. C*, **119**, No. 4: 1601 (2015); https://doi.org/10.1021/jp510606z
80. V.M. Nadutov, V.A. Tatarenko, and K.L. Tsinman, Statistical-Thermodynamic Analysis of Disorder–Order Structural Phase Transformations in F.C.C.-Fe–N Alloy, *Metallofizika*, **14**, No. 11: 42 (1992) (in Russian).
81. A.V. Ruban, Self-Trapping of Carbon Atoms in α-Fe during the Martensitic Transformation: A Qualitative Picture from ab initio Calculations, *Phys. Rev. B*, **90**, No. 14: 144106 (2014); https://doi.org/10.1103/PhysRevB.90.144106
82. E. Bain, The Nature of Martensite, *Trans. AIME*, **70**, 25 (1924).
83. G.V. Kurdjumov and G. Sachs, Über den Mechanismus der Stahlhärtung, *Z. Phys.*, **64**: 325 (1930) (in German); https://doi.org/10.1007/BF01397346
84. Y. Jiang, X. Zhang, A. Al Mehedi, M. Yang, and J.-P. Wang, A Method to Evaluate α″-$Fe_{16}N_2$ Volume Ratio in FeN Bulk Material by XPS, *Matter. Res. Express*, **2**, No. 11: 116103 (2015); https://doi.org/10.1088/2053-1591/2/11/116103
85. J. Li, W. Yuan, X. Peng, Y. Yang, J. Xu, X. Wang, B. Hong, H. Jin, D. Jin, and H. Ge, *AIP Advances*, **6**, No. 12: 125104 (2016); https://doi.org/10.1063/1.4967950
86. N. Ji, L.F. Allard, E. Lara-Curzio, and J.-P. Wang, N site Ordering Effect on Partially Ordered $Fe_{16}N_2$, *Appl. Phys. Lett.*, **98**, No. 9: 092506 (2011); https://doi.org/10.1063/1.3560051
87. Y. Hayashi and T. Sugeno, Nature of Boron in α-Iron, *Acta Metall.*, **18**, No. 6: 693 (1970); https://doi.org/10.1016/0001-6160(70)90099-4
88. R.B. McLellan, *Chemical Metallurgy of Iron and Steel* (London: Iron and Steel Institute: 1973), p. 337.
89. V.N. Bugaev and V.A. Tatarenko, *Interaction and Arrangement of Atoms in Interstitial Solid Solutions Based on Close-Packed Metals* (Kiev: Naukova Dumka: 1989) (in Russian).
90. V.G. Gavriljuk, V.M. Nadutov, and K. Ullakko, Low Temperature Ageing of Fe–N Martensite, *Scr. Met. Mater.*, **25**, No. 4: 905 (1991); https://doi.org/10.1016/0956-716X(91)90246-W
91. V.A. Tatarenko and K.L. Tsinman, Temperature- and Concentration-Dependent Tetragonality of a 'Hybrid' Binary Solution in Which Non-Metal Atoms Can Occupy Both Interstices and Sites of the B.C.T. Metal Lattice with Vacancies, *Metallofiz. Noveishie Tekhnol.*, **18**, No. 10: 32 (1996) (in Russian).
92. A.G. Khachaturyan, *Theory of Structural Transformations in Solids* (Mineola, New York: Dover Publications, Inc.: 2008).
93. V.A. Starenchenko, O.D. Pantyukhova, S.V. Starenchenko, and S.N. Kolupaeva, Mechanisms of Deformation-Induced Destruction of Long-Range Order Related to the Generation of Antiphase Boundaries and Point Defects in Alloys with the $L1_2$ Superstructure, *Phys. Met. Metallogr.*, **91**, No. 1: 85 (2001).
94. R.B. McLellan, The Thermodynamics of Hybrid Binary Interstitial–Substitutional Solid Solutions, *J. Phys. Chem. Solids*, **50**, No. 1: 49 (1989); https://doi.org/10.1016/0022-3697(89)90472-1

95. A. Udyansky, J. von Pezold, A. Dick, and J. Neugebauer, Orientational Ordering of Interstitial Atoms and Martensite Formation in Dilute Fe-Based Solid Solutions, *Phys. Rev. B*, 83, No. 18: 184112 (2011); https://doi.org/10.1103/PhysRevB.83.184112
96. A.G. Khachaturyan and G.A. Shatalov, Phase Transformation Associated with Radiation Defects, *Fiz. Tverdogo Tela*, **12**, No. 10: 2969 (1970) (in Russian).
97. M.A. Krivoglaz, *X-Ray and Neutron Diffraction in Nonideal Crystals* (Eds. (Berlin–Heidelberg: Springer: 1996); https://doi.org/10.1007/978-3-642-74291-0
98. V.A. Tatarenko and C.L. Tsinman, Strain-Induced and 'Blocking' Effects in Statistical Thermodynamics of 'Orientationally' Ordered Interstitial Solid Solutions, *Physics of Real Crystals* (Ed. V.G. Baryakhtar) (Kiev: Naukova Dumka: 1992), p. 244 (in Russian).
99. V.M. Nadutov, V.A. Tatarenko, C.L. Tsynman, and K. Ullakko, Interatomic Interaction and Atomic Ordering in Fe–N Martensite, *Metallofiz. Noveishie Tekhnol.*, **16**, No. 8: 34 (1994).
100. V.B. Molodkin, V.A. Tatarenko, and C.L. Tsinman, Influence of the Temperature Dependence of Static Displacements of Metal Ions on Diffraction Effects in an Ordered Nonstoichiometric Interstitial Phase Based on a B.C.C. Metal, *Metallofizika*, **15**, No. 9: 26 (1993) (in Russian).
101. L.A. Girifalco, *Statistical Physics of Materials* (New York: John Wiley and Sons: 1973).
102. I.M. Melnyk, T.M. Radchenko, and V.A. Tatarenko, Semi-Empirical Parameterization of Interatomic Interactions, Which is Based on Statistical-Thermodynamic Analysis of Data on Phase Equilibriums in B.C.C.-Fe–Co Alloy. I. Primary Ordering, *Metallofiz. Noveishie Tekhnol.*, **32**, No. 9: 1191 (2010) (in Ukrainian).
103. M.A. Krivoglaz, *Diffuse Scattering of X-Rays and Neutrons by Fluctuations* (Berlin–Heidelberg: Springer: 1996).
104. B.N. Brockhouse, H.E. Abou-Helal, and E.D. Hellman, Lattice Vibrations in Iron at 296 K, *Solid State Commun.*, **5**, No. 4: 211 (1967); https://doi.org/10.1016/0038-1098(67)90258-X
105. R. Kohlhaas, Ph. Dünner, and N. Schmitz-Pranghe, Uber die Temperaturabhangigkeit der Gitterparameter von Eisen, Kobalt und Nickel im Bereich Hoher Temperaturen, *Z. Angew. Phys.*, **23**, No. 4: 245 (1967) (in German).
106. J.A. Rayne and B.S. Chandrasekhar, Elastic Constants of Iron from 4.2 to 300 K, *Phys. Rev.*, **122**, No. 6: 1714 (1961); https://doi.org/10.1103/PhysRev.122.1714
107. D.J. Dever, Temperature Dependence of the Elastic Constants in α-Iron Single Crystals: Relationship to Spin Order and Diffusion Anomalies, *J. Appl. Phys.*, **43**, No. 8: 3293 (1972); https://doi.org/10.1063/1.1661710
108. L. Cheng, A. Boöttger, Th.H. de Keijser, and E.J. Mittemeijer, Lattice Parameters of Iron–Carbon and Iron–Nitrogen Martensites and Austenites, *Scr. Met. Mater.*, 24, No. 3: 509 (1990); https://doi.org/10.1016/0956-716X(90)90192-J
109. G.M. Stoica, A.D. Stoica, M.K. Miller, and D. Ma, Temperature-Dependent Elastic Anisotropy and Mesoscale Deformation in a Nanostructured Ferritic Alloy, *Nature Commun.*, **5**: 1 (2014); https://doi.org/10.1038/ncomms6178

110. Z.S. Basinski, W. Hume-Rothery, and A.L. Sutton, The Lattice Expansion of Iron, *Proc. R. Soc. Lond. A*, **229**: 459 (1955); https://doi.org/10.1098/rspa.1955.0102
111. W.G. Wolfer, Fundamental Properties of Defects in Metals, *Comprehensive Nuclear Materials* (Eds. R.J.M. Konings, T.R. Allen, R.E. Stoller, and Sh. Yamanaka) (Amsterdam–Kidlington–Oxford–Waltham: Elsevier Science: 2012), p. 1; https://doi.org/10.1016/B978-0-08-056033-5.00001-X
112. T.-S. Kuan, A. Warshel, and O. Schnepp, Intermolecular Potentials for N_2 Molecules and the Lattice Vibrations of Solid α-N_2, *J. Chem. Phys.*, **52**, No. 6: 3012 (1970); https://doi.org/10.1063/1.1673432
113. W.A. Harrison, *Pseudopotentials in the Theory of Metals* (New York: W.A. Benjamin Inc.: 1966).
114. W.A. Harrison, *Solid State Theory* (New York: Dover Publ. Inc.: 1979).
115. M.S. Blanter and A.G. Khachaturyan, Stress-Induced Interaction of Pairs of Point Defects in BCC Solutions, *Met. Trans. A*, **9**, No. 6: 753 (1978); https://doi.org/10.1007/BF02649784
116. E.S. Machlin, Pair Potential Model of Intermetallic Phases—I, *Acta Met.*, **22**, No. 1: 95 (1974); https://doi.org/10.1016/0001-6160(74)90129-1
117. L. Brewer, Prediction of High Temperature Metallic Phase Diagrams, *High-Strength Materials* (Ed. V.F. Zackay) (New York: John Wiley and Sons: 1965), Ch. 2, p. 12.
118. L. Brewer, *The Cohesive Energies of the Elements* (Rep. LBL-3720, Revised May 4, 1977) (Berkeley, CA, USA: Lawrence Berkeley Laboratory: 1977); https://escholarship.org/uc/item/08p2578m
119. V.G. Weizer and L.A. Girifalco, Vacancy–Vacancy Interaction in Copper, *Phys. Rev.*, **120**, No. 3: 837 (1960); https://doi.org/10.1103/PhysRev.120.837
120. R. Yamamoto and M.J. Doyama, The Interactions between Vacancies and Impurities in Metals by the Pseudopotential Method, *J. Phys. F: Met. Phys.*, **3**, No. 8: 1524 (1973); https://doi.org/10.1088/0305-4608/3/8/007
121. A.A. Smirnov, *Theory of Vacancies in Metals and Alloys and Its Applications to Substitutional Alloys* (Kiev: Naukova Dumka: 1993) (in Russian).
122. V.N. Bugaev, V.A. Tatarenko, and C.L. Tsinman, A Content of Site Vacancies in Binary Interstitial Alloys Based on F.C.C. Iron, *Metallofiz. Noveishie Tekhnol.*, **17**, No. 2: 32 (1995) (in Russian).

Received 17.11.2020;
in final version, 07.12.2020

Т.М. Радченко, О.С. Гаценко, В.В. Лізунов, В.А. Татаренко
Інститут металофізики ім. Г.В. Курдюмова НАН України,
бульв. Академіка Вернадського, 36, 03142 Київ, Україна

МАРТЕНСИТНА ФАЗА ТИПУ α''-$Fe_{16}N_2$ НЕСТЕХІОМЕТРИЧНОГО СКЛАДУ: НИНІШНІЙ СТАН ДОСЛІДЖЕНЬ І МІКРОСКОПІЧНИЙ СТАТИСТИЧНО-ТЕРМОДИНАМІЧНИЙ МОДЕЛЬ

Оглянуто та проаналізовано літературні (експериментальні та теоретичні) дані стосовно тетрагонального мартенситу з леґувальними елементами втілення–заміщення та вакансіями. Особливу увагу приділено вивченню мартенситної фази типу α''-$Fe_{16}N_2$ з унікальними та перспективними магнетними властивостями як альтернативи рідкісноземельним інтерметалідам і пермендюру на світовому ринку виробництва постійних магнетів. Охоплено період від часу відкриття її до нинішнього стану досліджень. Розвинуто статистично-термодинамічний модель «гібридного» твердого розчину втілення–заміщення на основі кристалічної ОЦТ-ґратниці, де леґувальні неметалеві компоненти (домішкові атоми) можуть займати як міжвузля, так і вакантні вузли ОЦК(Т)-ґратниці металу. Враховано дискретну (атомарно-кристалічну) будову ґратниці, анізотропію пружности, а також «блокувальні» та деформаційні (у тому числі «розмірні») ефекти у міжатомових взаємодіях. Модель адаптовано до максимально впорядкованої за типом α''-$Fe_{16}N_2$ нестехіометричної фази мартенситу Fe–N з атомами Нітроґену в октаедричних міжвузлях і на вузлах ОЦТ-заліза вище його температури Кюрі. Наголошено на важливості адекватного набору (залежних від температури та концентрації) наявних (у літературі) мікроскопічних енергетичних параметрів взаємодій атомів і вакансій. З'ясовано особливості змінення, а саме, немонотонного зменшення, за підвищення температури відносної концентрації атомів N в октаедричних міжвузлях ОЦТ-Fe, а тому й (корельованого з цією концентрацією) ступеня його тетрагональности. У широкому діяпазоні змінення загального вмісту втілених атомів N продемонстровано співвідношення рівноважної концентрації залишкових вузлових вакансій із концентрацією термічно активованих вакансій бездомішкового ОЦК-Fe за фіксованої температури.

Ключові слова: фаза α''-$Fe_{16}N_2$, мартенсит Fe–N, твердий розчин втілення–заміщення, тетрагональність, вакансії, упорядкування атомів, нерідкісноземельні магнетні матеріяли, постійні магнети.